

Molybdenum isotope evidence for extensive crustal extraction and recycling in Earth's first billion years

Alex J. McCoy-West^{1,2}, Priyadarshi Chowdhury², Kevin W. Burton¹, Paolo Sossi³, Geoff M. Nowell¹, J. Godfrey Fitton⁴, Andrew C. Kerr⁵, Peter A. Cawood² and Helen M. Williams^{1,6}

¹Department of Earth Sciences, Durham University, Elvet Hill, Durham DH1 3LE, UK

²School of Earth, Atmosphere and Environment, Monash University, Clayton, Victoria, 3800, Australia

³Institute of Geochemistry and Petrology, ETH Zürich

⁴School of GeoSciences, University of Edinburgh, Edinburgh EH9 3FE, UK

⁵School of Earth and Ocean Sciences, Cardiff University, Park Place, Cardiff CF10 3AT, UK

⁶Department of Earth Sciences, University of Cambridge, Downing Street, Cambridge CB2 3EQ, UK

Number of words: 3,029
Number of references: 49
Number of figures: 4
First paragraph (words): 151
Caption Length (words): 100, 96, 64, 90
Methods number of words: 1,190

Corresponding Author

Alex McCoy-West (alex.mccoywest@monash.edu)

School of Earth, Atmosphere and Environment, Monash University, Clayton, Victoria, 3800, Australia

1 **FIRST PARAGRAPH**

2 Estimates of the volume of the earliest crust based on zircon ages and radiogenic isotopes
3 remain equivocal. Stable isotope systems, such as molybdenum (Mo), have the potential to
4 provide further constraints but remain underused, due to the lack of complementarity between
5 mantle and crustal reservoirs. We present Mo isotope data for Archean komatiites and
6 Phanerozoic komatiites and picrites and demonstrate that their mantle sources all possess sub-
7 chondritic signatures complementary to the super-chondritic continental crust. These results
8 confirm that the present-day degree of mantle depletion was achieved by 3.5 billion years ago
9 and that the Earth has been in a steady state with respect to Mo recycling. Mass balance
10 modelling shows that this early mantle depletion requires the extraction of a far greater
11 volume of mafic-dominated proto-crust than previous thought, more than twice the volume of
12 the continental crust today, implying rapid crustal growth and destruction of crust in the first
13 billion years of Earth's history.

14 **MAIN TEXT**

15 The nature, extent and geodynamic settings of crustal formation and recycling are poorly
16 constrained, particularly during Hadean-early Archean times for which the rock-record is
17 scarce^{1,2}. The growth of the crust is estimated to be either temporally skewed with >60-80%
18 of the present-day volume of continental crust (PVCC) forming by 3 billion years ago (Ga)²⁻⁵,
19 or much more gradual with time^{1,6}. These growth curves are derived either from zircon
20 formation ages^{1,2} or from radiogenic isotopic evolution within the crust-mantle system⁶⁻⁸.
21 Zircon ages provide the lower bound on crustal growth as they cannot constrain the
22 magnitude of recycling. In contrast, growth curves of radiogenic isotope systems track the
23 evolution of mantle depletion and implicitly consider both crust extraction and recycling^{3,9}.
24 The complementarity of the crustal and mantle reservoirs for long-lived radiogenic isotopes
25 (Sr-Nd-Hf) has long been established, with time-dependent models requiring that only ~25-
26 50% of the mantle's mass underwent melt extraction to balance the present-day compositions
27 of the depleted mantle and crust^{7,8,10}. Estimating crustal growth from a mantle-depletion
28 perspective using time-invariant proxies provides an alternative approach⁴. The ratios of
29 stable isotopes being independent of time, fit this criterion and can put quantitative
30 constraints on differentiation processes occurring in the early Earth. However, this approach
31 is hindered by the lack of resolvable isotopic variation in samples representative of the
32 depleted mantle and crust for many non-traditional stable isotope systems.

33 Molybdenum stable isotopes ($\delta^{98}\text{Mo} = [({}^{98}\text{Mo}/{}^{95}\text{Mo}_{\text{sample}} / {}^{98}\text{Mo}/{}^{95}\text{Mo}_{\text{standard}}) - 1] \times$
34 1000; with the standard NIST3134 = 0‰) may be an exception, with a picture emerging of
35 two complementary reservoirs in the crust and mantle. Chondritic meteorites, the purported
36 building blocks of the terrestrial planets, have a relatively homogeneous average $\delta^{98}\text{Mo}$ of
37 $-0.154 \pm 0.013\text{‰}$ ^{11,12} (all errors on averages herein are 95% standard errors). Estimates of the

38 composition of the modern continental crust based on molybdenites, granites and primitive
39 arc-related basalts yield super-chondritic $\delta^{98}\text{Mo}$ values ranging from +0.05‰ to +0.3‰¹³⁻¹⁵.
40 If the bulk Earth is chondritic with respect to Mo stable isotopes and Mo is not fractionated
41 during its partitioning into Earth's core (cf. ¹⁶), then an isotopically light, sub-chondritic Mo
42 reservoir must exist in the mantle^{17,18}. Arc lavas show extremely variable $\delta^{98}\text{Mo}$ (-0.88‰ to
43 +0.24‰) but the consensus is that subduction zones appear to be fluxing isotopically light
44 Mo into the mantle¹⁹⁻²¹. However, whether this material is efficiently recycled or has enough
45 mass to affect the composition of the bulk mantle remains to be established. Previous Mo
46 isotope analyses of Archean komatiites¹⁷ have slightly sub-chondritic compositions, but
47 within error of chondrites¹¹, while five of the most depleted ($^{143}\text{Nd}/^{144}\text{Nd} > 0.5131$) mid-ocean
48 ridge basalts (MORB) measured are resolvably sub-chondritic²². Therefore, it is possible that
49 a complementary light sub-chondritic Mo isotope reservoir is present within the mantle¹⁸, but
50 its composition and nature remains poorly constrained.

51 Here, we focus on komatiite and picrite samples from four well characterized suites:
52 two from the Archean, the 3.5 Ga Komati (South Africa) and 2.7 Ga Munro (Canada)
53 komatiites²³, and two from the Phanerozoic, the 89 Ma Gorgona (Colombia) komatiites²⁴ and
54 the 61 Ma Baffin Island (NE Canada) picrites^{25,26}, to better constrain the Mo isotope
55 composition of the mantle throughout Earth's history. The selection of rock samples for this
56 purpose is non-trivial due to the complex behaviour of Mo during mantle melting. None of
57 the major mineral phases in the mantle host significant Mo²⁷, and the presence of residual
58 sulfides will strongly affect the Mo concentration of a melt owing given its chalcophile
59 nature¹⁸. Furthermore, isotopic studies of Mo isotopes in ultramafic lithologies are hampered
60 by the low concentration of Mo (<50 ng/g) and the significant isotopic variability in mantle
61 lithologies^{12,17}. Our studied ultramafic lavas formed at elevated temperatures (>1400 °C) by
62 high-degrees of partial melting (>25%), which would have lead to complete sulfide extraction

63 from their source regions²⁸, such that their Mo isotope compositions closely resemble that of
64 their mantle source regions. Our new results combined with the existing data are used to
65 constrain the $\delta^{98}\text{Mo}$ of the Earth's mantle, and subsequently global crustal volumes, during
66 Hadean-Archean times.

67

68 **ESTABLISHING A SUB-CHONDRITIC MO ISOTOPE RESERVIOR**

69 Our measurements show sub-chondritic values for unaltered Archean Komati and Munro
70 komatiites with $\delta^{98}\text{Mo}$ varying from -0.22 to -0.18‰ (Fig. 1; Table S1). Previous analyses
71 of Archean komatiites presented in Greber et al.¹⁷ define a wide range ($-0.32\text{‰} < \delta^{98}\text{Mo} <$
72 $+0.07\text{‰}$) with an average $\delta^{98}\text{Mo}$ of the four investigated localities calculated as -0.210
73 $\pm 0.098\text{‰}$. Combing these results is not straightforward. For example, previously analysed
74 samples from the Vetreny Belt, Fennoscandia have experienced significant crustal
75 assimilation²⁹ and consequently display resolvably heavier $\delta^{98}\text{Mo}$ ($-0.077 \pm 0.083\text{‰}$). We
76 thus disregard these samples in subsequent interpretations. In Greber et al.¹⁷, lavas from the
77 Komati Formation that were undoubtedly modified by alteration were excluded (Fig. 1;
78 $\delta^{98}\text{Mo}$ up to $+0.44\text{‰}$), but no further filtering for alteration was attempted. Given the high
79 mobility of Mo in fluids at low temperatures³⁰, we have filtered the Archean komatiite Mo
80 isotope data (Fig. S1), excluding samples that display major element mobility unrelated to
81 magmatic differentiation and are thus considered to have been modified by alteration (see
82 supplement). Our new data, along with the alteration-filtered dataset of ¹⁷, allows the
83 calculation of the $\delta^{98}\text{Mo}$ of Archean komatiites as $-0.199 \pm 0.019\text{‰}$.

84 Samples from the Phanerozoic Gorgona komatiites, the freshest komatiite occurrence
85 in the world, have a restricted range of $\delta^{98}\text{Mo}$ from -0.18 to -0.25‰ and yield an average
86 $\delta^{98}\text{Mo}$ of $-0.207 \pm 0.034\text{‰}$, which is within error of their Archean equivalents. In contrast,

87 the Phanerozoic Baffin Island picrites possess variable $\delta^{98}\text{Mo}$ from -0.13 to -0.32‰ , which
88 at first glance suggests a lighter composition (Fig. 1). However, the Baffin Island picrites
89 represent a special case of disequilibrium olivine accumulation²⁶ and after correction the
90 composition of the parental melt is calculated as $\delta^{98}\text{Mo} = -0.210 \pm 0.010\text{‰}$ (Table S2). The
91 $\delta^{98}\text{Mo}$ of the Baffin Island parental melts are thus within error of depleted MORB²², the
92 Gorgona komatiites, and three Archean komatiite localities that span 800 Ma, suggesting that
93 the Mo isotope composition of the accessible mantle has changed little over the last 3.5 Ga.
94 These data for magmatic rocks are augmented by mantle xenoliths to calculate the average
95 composition of the depleted mantle as $\delta^{98}\text{Mo} = -0.204 \pm 0.008\text{‰}$ (Table S3).

96 These results place several new constraints on the evolution of Earth's mantle,
97 notably: 1) the Mo isotope composition of the accessible mantle is unambiguously sub-
98 chondritic (an analysis of variance test confirms that the mantle samples are a resolvably
99 different population to chondritic meteorites at the 99% significance level; p-value <0.001);
100 2) the formation of this reservoir must have occurred before ~ 3.5 Ga, 3) it must have had a
101 substantial volume (magmas generated at a range of melting depths are affected); and 4) no
102 resolvable temporal variations are observed with Archean komatiites ranging in age from
103 3.5–2.7 Ga having identical $\delta^{98}\text{Mo}$ to Cretaceous Gorgona komatiites and Paleogene Baffin
104 Island picrites and modern MORB (an analysis of variance test confirms that the means of
105 these populations are identical; p-value ~ 0.42). Together these constraints demonstrate that
106 most of the present-day depletion of the mantle must have been completed by the
107 Paleoproterozoic. This finding is in agreement with independent constraints on the temporal
108 chemical evolution of continental basalts, which indicates a nearly constant amount of mantle
109 depletion since ~ 3.8 Ga³¹. However, the amount of mantle depletion, and hence the volume
110 of early continental crust produced and subsequently destroyed, remain under-constrained^{3,9}.
111 Nonetheless, most studies agree that 30–50% melt depletion of the whole mantle can

112 reproduce most of the radiogenic and incompatible element signatures of the crust and
113 depleted mantle, assuming they represent complementary reservoirs^{7,8,10}. This has significant
114 implications for the growth of early crust given that the proto-crust and depleted mantle
115 should chemically complement each other, if no other processes have perturbed the system.
116 We explore this further below.

117 **COMPOSITION OF THE SILICATE EARTH**

118 Due to the refractory nature of Mo in the solar nebula, we assume that the proto-Earth
119 inherited the $\delta^{98}\text{Mo}$ of chondritic meteorites (Fig. 2). Soon after accretion, core formation
120 occurred ($\approx 34 \text{ Ma}^{32}$) resulting in the efficient removal of the highly siderophile elements into
121 the Fe-Ni metal core, including 95% of the Earth's original Mo^{33} (Table S5). The near
122 quantitative removal of Mo to the core means isotope ratios in the metallic phase are unlikely
123 to be fractionated from those in bulk chondrites, as observed in iron meteorites¹¹. Early
124 experimental work suggested this sequestration of Mo may have been associated with a small
125 but resolvable isotopic fractionation of the silicate portion of the planet³⁴. However, recent
126 metal-silicate experiments which incorporate the effect of Mo valence state¹⁶ suggest a
127 significantly reduced $\Delta^{98}\text{Mo}_{\text{metal-silicate}}$ of as little as -0.008‰ (assuming $\text{Mo}^{6+}/\sum\text{Mo} = 0.1$; T
128 $= 2500 \text{ °C}$), which means the mantle would remain within the error of the composition of
129 chondrites following core formation. Subsequent modification of the residual bulk silicate
130 Earth (BSE) may have occurred during: 1) the Moon-forming impact: where an planet-sized
131 body impacted Earth and added volatiles, including significant sulfur, which were then
132 sequestered to the outer core in the "Hadean matte" ($<1\%$ of core mass; this sulfide-enriched
133 phase is expected to have preferentially incorporated isotopically light $\text{Mo}^{35,36}$); or 2) late
134 accretion: since geochemical modelling suggests that all of the Mo in Earth's mantle was
135 added during the last 10% of accretion³⁷, with N -body simulations require only $\sim 1\%$ of the

136 Earth's mass was accreted following the Moon-forming impact³⁸. Ultimately, due to the
137 chondritic composition of the new materials these processes will not significantly change the
138 $\delta^{98}\text{Mo}$ of the BSE, which should be around $\delta^{98}\text{Mo} \approx -0.154\text{‰}$. Therefore, the only
139 remaining global-scale mechanism that can modify the Earth's Mo isotope budget and
140 account for the Earth's super-chondritic crust and sub-chondritic mantle is the extraction of
141 the crust (Fig. 2). Furthermore, the presence of positive Nb anomalies and radiogenic Nd
142 isotope compositions in some komatiite suites suggest that their source regions have
143 previously undergone melt extraction²³.

144 **EXTRACTION OF AN ISOTOPICALLY HEAVY CRUST**

145 The sub-chondritic mantle $\delta^{98}\text{Mo}$ signature may be the result of partial melting²² or
146 continental crust extraction¹⁷ or both, but the exact magnitude of fractionation remains
147 uncertain. Here we have developed a partial melting model to assess the direction and
148 magnitude of fractionation of $\delta^{98}\text{Mo}$ between melt and residual mantle (Fig. 3). This
149 modelling demonstrates several important points: 1) high-MgO partial melts are accurate
150 recorders of the Mo isotope composition of their mantle sources because at high temperatures
151 $\Delta^{98}\text{Mo}_{\text{melt-solid}} < 0.012\text{‰}$ at 30% melting (Fig. 3a); 2) melting of a chondritic reservoir to form
152 basalt reproduces the average basalt used in modelling ($\delta^{98}\text{Mo} = -0.10\text{‰}$) with ~12%
153 melting at 1300 °C. This ~0.05‰ difference in $\delta^{98}\text{Mo}$ is comparable to that observed between
154 N-MORB²² and the depleted mantle composition (herein); 3) the composition of modern
155 upper continental crust or Phanerozoic granites (Fig. 1; $\Delta^{98}\text{Mo}_{\text{granite-mantle}} +0.36\text{‰}$) cannot be
156 generated by direct melting of the mantle. The majority of the enrichment of these samples in
157 heavy $\delta^{98}\text{Mo}$ must instead result from intracrustal differentiation, either through the addition
158 of isotopically heavy subduction zone fluids¹⁹ or hydrothermal fluids³⁹ or the removal of
159 isotopically light hydrous phases (biotite or amphibole)¹³ into cumulates in the lower crust.

160 Molybdenum isotope fractionation during melt extraction may be driven by both
161 changes in Mo oxidation state and co-ordination number. Given that Mo^{6+} is significantly
162 more incompatible than Mo^{4+27} residues of melting will have lower $\text{Mo}^{6+}/\Sigma\text{Mo}$ than melt in
163 addition to higher mean co-ordination number, and hence will display lighter $\delta^{98}\text{Mo}$
164 consistent with sense of fractionation observed in the komatiites measured herein (Fig. 1).
165 The oxidation state of Mo in the modern mantle remains uncertain, however, partitioning
166 studies indicate Mo is predominantly hexavalent in melts at typical upper mantle conditions
167 ($\text{Mo}^{6+}/\Sigma\text{Mo} \approx 0.99^{16,27,40}$). Although mantle oxygen fugacity is generally considered to have
168 been constant for the last ~ 3.5 Ga⁴¹, recent work using V partitioning provides strong
169 evidence of increasing oxygen fugacity with time⁴², therefore here we impose $\text{Mo}^{6+}/\Sigma\text{Mo} =$
170 0.95 for early mantle melting (Fig. 3b). Creation of felsic components of the Hadean-
171 Eoarchean crust such as tonalite-trondhjemite-granodiorite (TTG) granitoids, requires
172 remelting of metabasalt (mafic amphibolite)⁴³, which will further enrich this felsic component
173 in heavier isotopes by up to 0.08‰ (at 900 °C and $F = 20\%$), but cannot explain the full range
174 of heavy $\delta^{98}\text{Mo}$ observed. The models presented here evaluate mantle melting only and
175 should be considered minimum estimates and approximate until Mo isotope fractionation
176 factors can be independently determined for accessory phases that may retain isotopically
177 light Mo (e.g. garnet, amphibole, sulfide). Nonetheless, they demonstrate that there is no need
178 to invoke subduction zone processes in the early Earth to form the mafic crusts discussed
179 below, which can instead be generated solely through mantle melting processes.

180 **EXTENSIVE EXTRACTION AND RECYCLING OF EARLY CRUST**

181 Assuming a two-reservoir model involving a proto-crust(C) and depleted mantle(DM), we
182 have estimated the crustal volume that is required to have formed by ~ 3.5 Ga to reconcile the

183 $\delta^{98}\text{Mo}$ and Mo-concentration of the mantle that sourced the Archean komatiites using the
184 mass-balance equation:

$$m_C = \frac{m_{DM} \cdot [Mo]_{DM} \cdot (\delta_{BSE}^{98} - \delta_{DM}^{98})}{[Mo]_C \cdot (\delta_C^{98} - \delta_{BSE}^{98})}$$

185 where m_i , $[Mo]_i$ and δ_i^{98} represents the mass, Mo concentration and Mo isotope
186 composition, respectively, of the various reservoirs. It is important to note the mass balance
187 modelling presented here does not reflect the instantaneous removal of melts from the mantle,
188 but rather the effect of the time-integrated isolation of the proto-crust from the convecting
189 mantle.

190 Calculations of continental growth based on the zircon archive and mantle depletion
191 commonly use the present-day continental crust as the crustal endmember. However, there
192 are two major compositional differences between the early continents and their modern
193 analogues^{2,8}. These are: 1) TTG granitoids were the dominant felsic rocks with true potassic
194 (K) granites subordinate in abundance⁴³ and, 2) mafic lithologies were more abundant than
195 their felsic counterparts^{44,45}. Here we assume the BSE had an initial $\delta^{98}\text{Mo}$ equal to chondritic
196 meteorites (for alternate scenarios Fig. S6) and have investigated two scenarios to encompass
197 the variability of $\delta^{98}\text{Mo}$ in Archean felsic rocks (granites or TTGs represent the felsic
198 endmember; Fig. 4). These scenarios thus provide the minimum and maximum estimates of
199 the extent of pre-3.5 Ga crust extraction. We have then calculated crustal volumes for three
200 different model proto-crusts: a hypothetical purely felsic crust, Mafic crust-A (minimum
201 based on a mafic crust) and Mafic crust-B (a likely Eoarchean crustal composition).
202 Calculations based on the purely felsic crusts suggest a minimum of 0.5-1.5 times the PVCC
203 ($\sim 7.2 \times 10^9 \text{ km}^3$) existed prior to 3.5 Ga based on 30 % depletion of the whole mantle (Fig. 4).
204 This range is consistent with the growth model calculated using Nb/U ratios of the crust-

205 mantle system⁴, but is higher than those calculated using the crustal zircon formation ages
206 (<50% of PVCC at 3.5 Ga;²). This suggests that time-invariant proxies of mantle depletion
207 record similar volumes of early crust extraction, whereas their difference with the zircon-
208 based models reflects the influence of crustal recycling. More realistic calculations based on
209 dominantly mafic crust types require crustal volumes greater than the PVCC by ~3.5 Ga (Fig
210 4). For example, in the preferred Eoarchean scenario with a TTG felsic component the
211 crustal volumes based on Mafic crust-A and -B will be 2.5 and 3.8 times the PVCC,
212 respectively, assuming the minimum likely amount of mantle depletion (30%;^{7,8,10}; Fig. 4b).
213 These higher values are mostly a consequence of the lower Mo concentration (and to a minor
214 extent the lighter isotopic compositions) of these model crusts (see Table S5). It is debatable
215 whether to consider dominantly mafic crust as continental or not^{44,45}, but our calculations
216 show that even the volume of a hypothetical TTG crust would have been greater than the
217 PVCC, provided the depleted mantle size exceeds ~20% of the whole mantle. Thus, it is
218 highly likely that a greater volume of crust than the PVCC was extracted in the first billion
219 years of Earth's history, most of which was then subsequently recycled into the mantle.

220 Large-scale crust extraction is consistent with the prediction of voluminous melting of
221 the mantle owing to its hotter thermal structure during Hadean-Archean times⁴⁶. However,
222 our calculated crustal volumes represent the amount of crust extracted from the mantle and
223 not its net growth, which is determined by the difference between extracted (generated) and
224 recycled volumes of the crust⁹. Nevertheless, high rates of crust formation should result in
225 rapid crustal growth unless the recycling rates equal or exceed extraction rates. Several
226 independent continental growth models^{2,3,5} do suggest extremely rapid continental growth
227 consistent with the idea that extensive crust formation may have happened on the early Earth.
228 Given the dearth of such old rocks in the present rock record, it is unequivocal that much of
229 the >3.5 Ga crust has been recycled. Mantle-derived isotopic heterogeneities are widespread

230 in modern basalts, reflecting sluggish mantle mixing. Modelling of stagnant lid regimes
231 shows that mixing was up to an order of magnitude slower under these conditions⁴⁷ therefore
232 it is expected that this recycled crustal material will not have mixed back completely into the
233 accessible mantle. Although difficult to constrain, recent studies on Archean continental
234 recycling^{48,49} suggest extensive recycling (but not exceeding the formation rates) of the crust,
235 with a volume equivalent to the PVCC probably recycled during the late Archean⁴⁸. If the
236 recycling rates were similar during most of the Hadean-Archean, twice the PVCC could have
237 been recycled back into the mantle during that period. Consequently, we have not only been
238 significantly underestimating the volumes of early formed crust, but also the amount of
239 material that was being recycled back into the mantle.

240

241 **Acknowledgements**

242 Dave Selby is thanked for access to carius tube facilities. This project was funded by a
243 European Research Council Starting Grant (“HabitablePlanet” 306655) to HMW and a
244 NERC Grant (NE/M0003/1) to KWB. While at Monash AMW, PC and PAC were supported
245 by ARC grant FL160100168.

246

247 **Author Contributions**

248 AMW and HMW conceived the study. AMW undertook the chemistry and mass
249 spectrometry with assistance from GMN. JGF, ACK and PS provided the samples. AMW and
250 PC developed the mass balance modelling. AMW and PS developed the Mo isotope partial
251 melting model. All authors contributed to discussions on early crustal volumes and writing
252 and editing the paper.

253

254

255

256 REFERENCES

- 257 1 Condie, K. C. Episodic continental growth and supercontinents: a mantle avalanche connection? *Earth*
258 *and Planetary Science Letters* **163**, 97-108 (1998).
- 259 2 Dhuime, B., Hawkesworth, C. J., Cawood, P. A. & Storey, C. D. A change in the geodynamics of
260 continental growth 3 billion years ago. *Science* **335**, 1334-1336, doi:10.1126/science.1216066 (2012).
- 261 3 Korenaga, J. Estimating the formation age distribution of continental crust by unmixing zircon ages.
262 *Earth and Planetary Science Letters* **482**, 388-395, doi:<https://doi.org/10.1016/j.epsl.2017.11.039>
263 (2018).
- 264 4 Campbell, I. H. Constraints on continental growth models from Nb/U ratios in the 3.5 Ga Barberton
265 and other Archaean basalt-komatiite suites. *American Journal of Science* **303**, 319-351,
266 doi:10.2475/ajs.303.4.319 (2003).
- 267 5 Armstrong, R. L. Radiogenic isotopes: the case for crustal recycling on a near-steady-state no-
268 continental-growth Earth. *Philosophical Transactions of the Royal Society of London* **301**, 443-472,
269 doi:10.1098/rsta.1981.0122 (1981).
- 270 6 McCulloch, M. T. & Bennett, V. C. Progressive growth of the Earth's continental crust and depleted
271 mantle: Geochemical constraints. *Geochimica et Cosmochimica Acta* **58**, 4717-4738,
272 doi:[http://dx.doi.org/10.1016/0016-7037\(94\)90203-8](http://dx.doi.org/10.1016/0016-7037(94)90203-8) (1994).
- 273 7 DePaolo, D. J. Crustal growth and mantle evolution: inferences from models of element transport and
274 Nd and Sr isotopes. *Geochimica et Cosmochimica Acta* **44**, 1185-1196,
275 doi:[https://doi.org/10.1016/0016-7037\(80\)90072-1](https://doi.org/10.1016/0016-7037(80)90072-1) (1980).
- 276 8 Jacobsen, S. B. Isotopic and chemical constraints on mantle-crust evolution. *Geochimica et*
277 *Cosmochimica Acta* **52**, 1341-1350, doi:[https://doi.org/10.1016/0016-7037\(88\)90205-0](https://doi.org/10.1016/0016-7037(88)90205-0) (1988).
- 278 9 Cawood, P. A., Hawkesworth, C. J. & Dhuime, B. The continental record and the generation of
279 continental crust. *GSA Bulletin* **125**, 14-32, doi:10.1130/B30722.1 (2013).
- 280 10 O'Nions, R. K., Evensen, N. M. & Hamilton, P. J. Geochemical modeling of mantle differentiation and
281 crustal growth. *Journal of Geophysical Research: Solid Earth* **84**, 6091-6101,
282 doi:doi:10.1029/JB084iB11p06091 (1979).
- 283 11 Burkhardt, C., Hin, R. C., Kleine, T. & Bourdon, B. Evidence for Mo isotope fractionation in the solar
284 nebula and during planetary differentiation. *Earth and Planetary Science Letters* **391**, 201-211,
285 doi:<http://dx.doi.org/10.1016/j.epsl.2014.01.037> (2014).
- 286 12 Liang, Y.-H. *et al.* Molybdenum isotope fractionation in the mantle. *Geochimica et Cosmochimica*
287 *Acta* **199**, 91-111, doi:<https://doi.org/10.1016/j.gca.2016.11.023> (2017).
- 288 13 Voegelin, A. R., Pettke, T., Greber, N. D., von Niederhäusern, B. & Nägler, T. F. Magma
289 differentiation fractionates Mo isotope ratios: Evidence from the Kos Plateau Tuff (Aegean Arc).
290 *Lithos* **190-191**, 440-448, doi:<http://dx.doi.org/10.1016/j.lithos.2013.12.016> (2014).
- 291 14 Yang, J. *et al.* The molybdenum isotopic compositions of I-, S- and A-type granitic suites. *Geochimica*
292 *et Cosmochimica Acta* **205**, 168-186, doi:<https://doi.org/10.1016/j.gca.2017.01.027> (2017).
- 293 15 Greber, N. D., Pettke, T. & Nägler, T. F. Magmatic-hydrothermal molybdenum isotope fractionation
294 and its relevance to the igneous crustal signature. *Lithos* **190-191**, 104-110,
295 doi:<https://doi.org/10.1016/j.lithos.2013.11.006> (2014).
- 296 16 Hin, R. C., Burnham, A. D., Gianolio, D., Walter, M. J. & Elliott, T. Molybdenum isotope fractionation
297 between Mo⁴⁺ and Mo⁶⁺ in silicate liquid and metallic Mo. *Chemical Geology* **504**, 177-189,
298 doi:<https://doi.org/10.1016/j.chemgeo.2018.11.014> (2019).
- 299 17 Greber, N. D., Puchtel, I. S., Nägler, T. F. & Mezger, K. Komatiites constrain molybdenum isotope
300 composition of the Earth's mantle. *Earth and Planetary Science Letters* **421**, 129-138,
301 doi:<https://doi.org/10.1016/j.epsl.2015.03.051> (2015).
- 302 18 Willbold, M. & Elliott, T. Molybdenum isotope variations in magmatic rocks. *Chemical Geology* **449**,
303 253-268, doi:<https://doi.org/10.1016/j.chemgeo.2016.12.011> (2017).
- 304 19 Freymuth, H., Vils, F., Willbold, M., Taylor, R. N. & Elliott, T. Molybdenum mobility and isotopic
305 fractionation during subduction at the Mariana arc. *Earth and Planetary Science Letters* **432**, 176-186,
306 doi:<http://dx.doi.org/10.1016/j.epsl.2015.10.006> (2015).
- 307 20 Gaschnig, R. M. *et al.* The Molybdenum Isotope System as a Tracer of Slab Input in Subduction
308 Zones: An Example From Martinique, Lesser Antilles Arc. *Geochemistry, Geophysics, Geosystems* **18**,
309 4674-4689, doi:doi:10.1002/2017GC007085 (2017).
- 310 21 König, S., Wille, M., Voegelin, A. & Schoenberg, R. Molybdenum isotope systematics in subduction
311 zones. *Earth and Planetary Science Letters* **447**, 95-102, doi:<https://doi.org/10.1016/j.epsl.2016.04.033>
312 (2016).
- 313 22 Bezar, R., Fischer-Gödde, M., Hamelin, C., Brenneka, G. A. & Kleine, T. The effects of magmatic
314 processes and crustal recycling on the molybdenum stable isotopic composition of Mid-Ocean Ridge

315 Basalts. *Earth and Planetary Science Letters* **453**, 171-181,
316 doi:<http://dx.doi.org/10.1016/j.epsl.2016.07.056> (2016).

317 23 Sossi, P. A. *et al.* Petrogenesis and Geochemistry of Archean Komatiites. *Journal of Petrology* **57**, 147-
318 184, doi:10.1093/petrology/egw004 (2016).

319 24 Kerr, A. C. *et al.* The petrogenesis of Gorgona komatiites, picrites and basalts: new field, petrographic
320 and geochemical constraints. *Lithos* **37**, 245-260, doi:[http://dx.doi.org/10.1016/0024-4937\(95\)00039-9](http://dx.doi.org/10.1016/0024-4937(95)00039-9)
321 (1996).

322 25 Starkey, N. A. *et al.* Helium isotopes in early Iceland plume picrites: Constraints on the composition of
323 high ³He/⁴He mantle. *Earth and Planetary Science Letters* **277**, 91-100,
324 doi:<https://doi.org/10.1016/j.epsl.2008.10.007> (2009).

325 26 McCoy-West, A. J., Godfrey Fitton, J., Pons, M.-L., Inglis, E. C. & Williams, H. M. The Fe and Zn
326 isotope composition of deep mantle source regions: Insights from Baffin Island picrites. *Geochimica et*
327 *Cosmochimica Acta* **238**, 542-562, doi:<https://doi.org/10.1016/j.gca.2018.07.021> (2018).

328 27 Leitzke, F. P. *et al.* Redox dependent behaviour of molybdenum during magmatic processes in the
329 terrestrial and lunar mantle: Implications for the Mo/W of the bulk silicate Moon. *Earth and Planetary*
330 *Science Letters* **474**, 503-515, doi:<https://doi.org/10.1016/j.epsl.2017.07.009> (2017).

331 28 McCoy-West, A. J., Bennett, V. C., O'Neill, H. S. C., Hermann, J. & Puchtel, I. S. The interplay
332 between melting, refertilization and carbonatite metasomatism in off-cratonic lithospheric mantle under
333 Zealandia: An integrated major, trace and platinum group element study. *Journal of Petrology* **56**, 563-
334 604, doi:10.1093/petrology/egv011 (2015).

335 29 Puchtel, I. S. *et al.* Petrology of a 2.41 Ga remarkably fresh komatiitic basalt lava lake in Lion Hills,
336 central Vetryny Belt, Baltic Shield. *Contributions to Mineralogy and Petrology* **124**, 273-290,
337 doi:10.1007/s004100050191 (1996).

338 30 Keppler, H. & Wyllie, P. J. Partitioning of Cu, Sn, Mo, W, U, and Th between melt and aqueous fluid
339 in the systems haplogranite-H₂O-HCl and haplogranite-H₂O-HF. *Contributions to Mineralogy and*
340 *Petrology* **109**, 139-150, doi:10.1007/bf00306474 (1991).

341 31 Keller, B. & Schoene, B. Plate tectonics and continental basaltic geochemistry throughout Earth
342 history. *Earth and Planetary Science Letters* **481**, 290-304,
343 doi:<https://doi.org/10.1016/j.epsl.2017.10.031> (2018).

344 32 Kleine, T. & Walker, R. J. Tungsten Isotopes in Planets. *Annual Review of Earth and Planetary*
345 *Sciences* **45**, 389-417, doi:10.1146/annurev-earth-063016-020037 (2017).

346 33 McDonough, W. F. in *Treatise on Geochemistry (First Edition)* Vol. 2 (eds Heinrich D. Holland &
347 Karl K. Turekian) 547-568 (Elsevier, 2003).

348 34 Hin, R. C., Burkhardt, C., Schmidt, M. W., Bourdon, B. & Kleine, T. Experimental evidence for Mo
349 isotope fractionation between metal and silicate liquids. *Earth and Planetary Science Letters* **379**, 38-
350 48, doi:<http://dx.doi.org/10.1016/j.epsl.2013.08.003> (2013).

351 35 Savage, P. S. *et al.* Copper isotope evidence for large-scale sulphide fractionation during Earth's
352 differentiation. *Geochemical Perspectives Letters* **1**, 53-64,
353 doi:<http://dx.doi.org/10.7185/geochemlet.1506> (2015).

354 36 McCoy-West, A. J., Millet, M.-A. & Burton, K. W. The neodymium stable isotope composition of the
355 silicate Earth and chondrites. *Earth and Planetary Science Letters* **480**, 121-132,
356 doi:<https://doi.org/10.1016/j.epsl.2017.10.004> (2017).

357 37 Dauphas, N. The isotopic nature of the Earth's accreting material through time. *Nature* **541**, 521,
358 doi:10.1038/nature20830
359 <https://www.nature.com/articles/nature20830#supplementary-information> (2017).

360 38 Jacobson, S. A. *et al.* Highly siderophile elements in Earth's mantle as a clock for the Moon-forming
361 impact. *Nature* **508**, 84, doi:10.1038/nature13172 (2014).

362 39 Neely, R. A. *et al.* Molybdenum isotope behaviour in groundwaters and terrestrial hydrothermal
363 systems, Iceland. *Earth and Planetary Science Letters* **486**, 108-118,
364 doi:<https://doi.org/10.1016/j.epsl.2017.11.053> (2018).

365 40 O'Neill, H. S. C. & Eggins, S. M. The effect of melt composition on trace element partitioning: an
366 experimental investigation of the activity coefficients of FeO, NiO, CoO, MoO₂ and MoO₃ in silicate
367 melts. *Chemical Geology* **186**, 151-181, doi:[http://dx.doi.org/10.1016/S0009-2541\(01\)00414-4](http://dx.doi.org/10.1016/S0009-2541(01)00414-4) (2002).

368 41 Hibbert, K. E. J., Williams, H. M., Kerr, A. C. & Puchtel, I. S. Iron isotopes in ancient and modern
369 komatiites: Evidence in support of an oxidised mantle from Archean to present. *Earth and Planetary*
370 *Science Letters* **321-322**, 198-207, doi:<http://dx.doi.org/10.1016/j.epsl.2012.01.011> (2012).

371 42 Nicklas, R. W. *et al.* Secular mantle oxidation across the Archean-Proterozoic boundary: Evidence
372 from V partitioning in komatiites and picrites. *Geochimica et Cosmochimica Acta* **250**, 49-75,
373 doi:<https://doi.org/10.1016/j.gca.2019.01.037> (2019).

374 43 Moyen, J.-F. & Laurent, O. Archaean tectonic systems: A view from igneous rocks. *Lithos* **302-303**,
375 99-125, doi:<https://doi.org/10.1016/j.lithos.2017.11.038> (2018).

376 44 Dhuime, B., Wuestefeld, A. & Hawkesworth, C. J. Emergence of modern continental crust about 3
377 billion years ago. *Nature Geoscience* **8**, 552, doi:10.1038/ngeo2466
378 <https://www.nature.com/articles/ngeo2466#supplementary-information> (2015).

379 45 Tang, M., Chen, K. & Rudnick, R. L. Archean upper crust transition from mafic to felsic marks the
380 onset of plate tectonics. *Science* **351**, 372-375, doi:10.1126/science.aad5513 (2016).

381 46 Herzberg, C., Condie, K. & Korenaga, J. Thermal history of the Earth and its petrological expression.
382 *Earth and Planetary Science Letters* **292**, 79-88, doi:<https://doi.org/10.1016/j.epsl.2010.01.022> (2010).

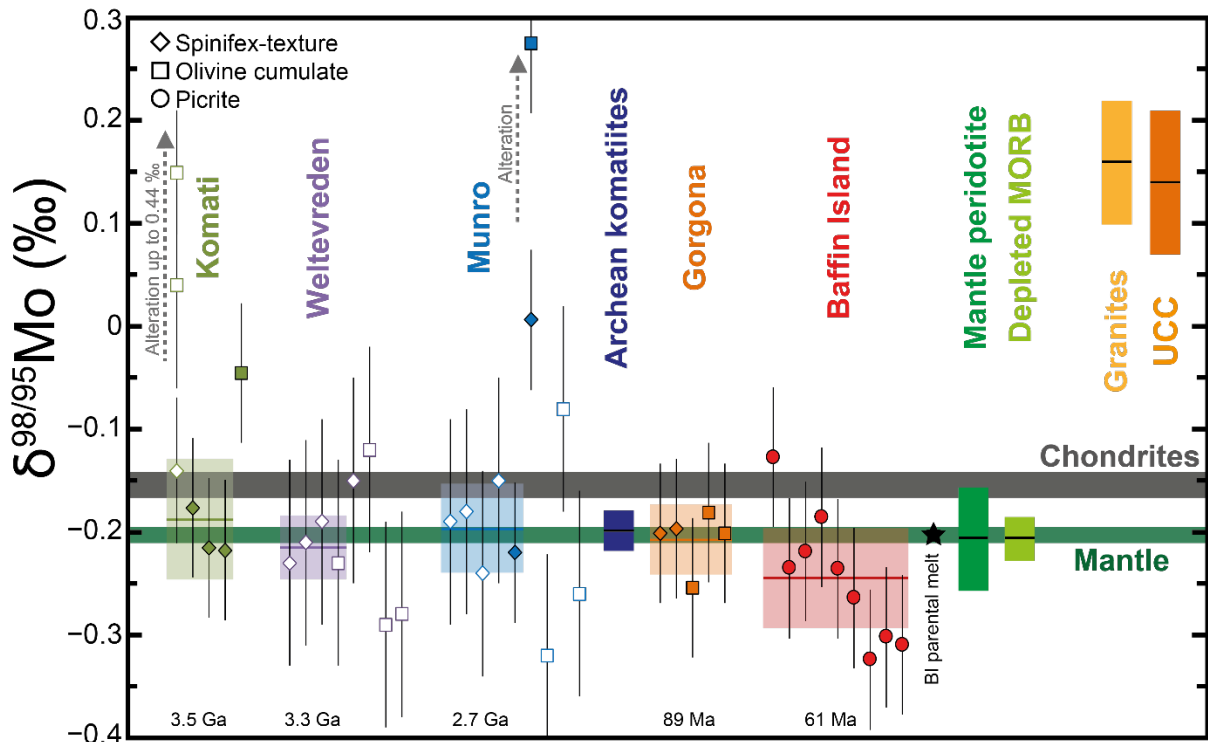
383 47 O'Neill, C., Debaille, V. & Griffin, W. Deep earth recycling in the Hadean and constraints on surface
384 tectonics. *American Journal of Science* **313**, 912-932, doi:10.2475/09.2013.04 (2013).

385 48 Chowdhury, P., Gerya, T. & Chakraborty, S. Emergence of silicic continents as the lower crust peels
386 off on a hot plate-tectonic Earth. *Nature Geoscience* **10**, 698, doi:10.1038/ngeo3010
387 <https://www.nature.com/articles/ngeo3010#supplementary-information> (2017).

388 49 Johnson, T. E., Brown, M., Kaus, B. J. P. & VanTongeren, J. A. Delamination and recycling of
389 Archaean crust caused by gravitational instabilities. *Nature Geoscience* **7**, 47, doi:10.1038/ngeo2019
390 <https://www.nature.com/articles/ngeo2019#supplementary-information> (2013).

391

392

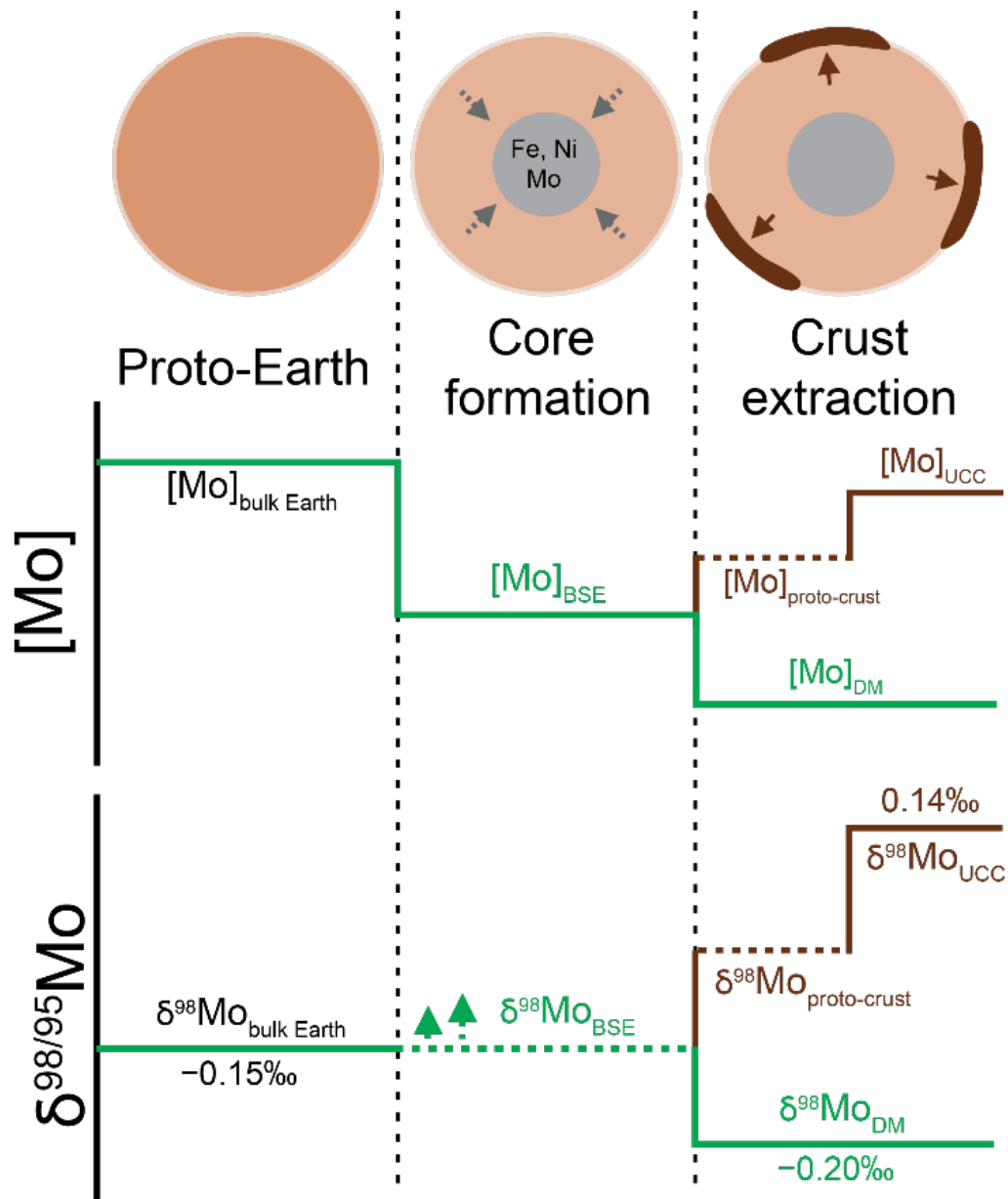


396 **Figure 1:** Variation of $\delta^{98}\text{Mo}$ in komatiites, picrites and major mantle and crustal reservoirs.

397 Filled symbols are data analysed herein with hollow symbols data taken from Greber et al. ¹⁷.

398 All individual analyses are plotted with the 2 standard deviation long term error, with the
 399 shaded areas for different formations and reservoirs the being 95% standard errors. The dark
 400 grey band represents chondritic meteorites ($\delta^{98}\text{Mo} = -0.154 \pm 0.013\text{‰}$; ^{11,12}) with the green
 401 bar representing the resolvable lighter depleted mantle ($\delta^{98}\text{Mo} = -0.204 \pm 0.008\text{‰}$; herein).

402 Average Archean komatiites ($\delta^{98}\text{Mo} = -0.199 \pm 0.019\text{‰}$; herein) with other reservoirs from
 403 ^{12,14,22} (see Table S3).



404

405

406

407

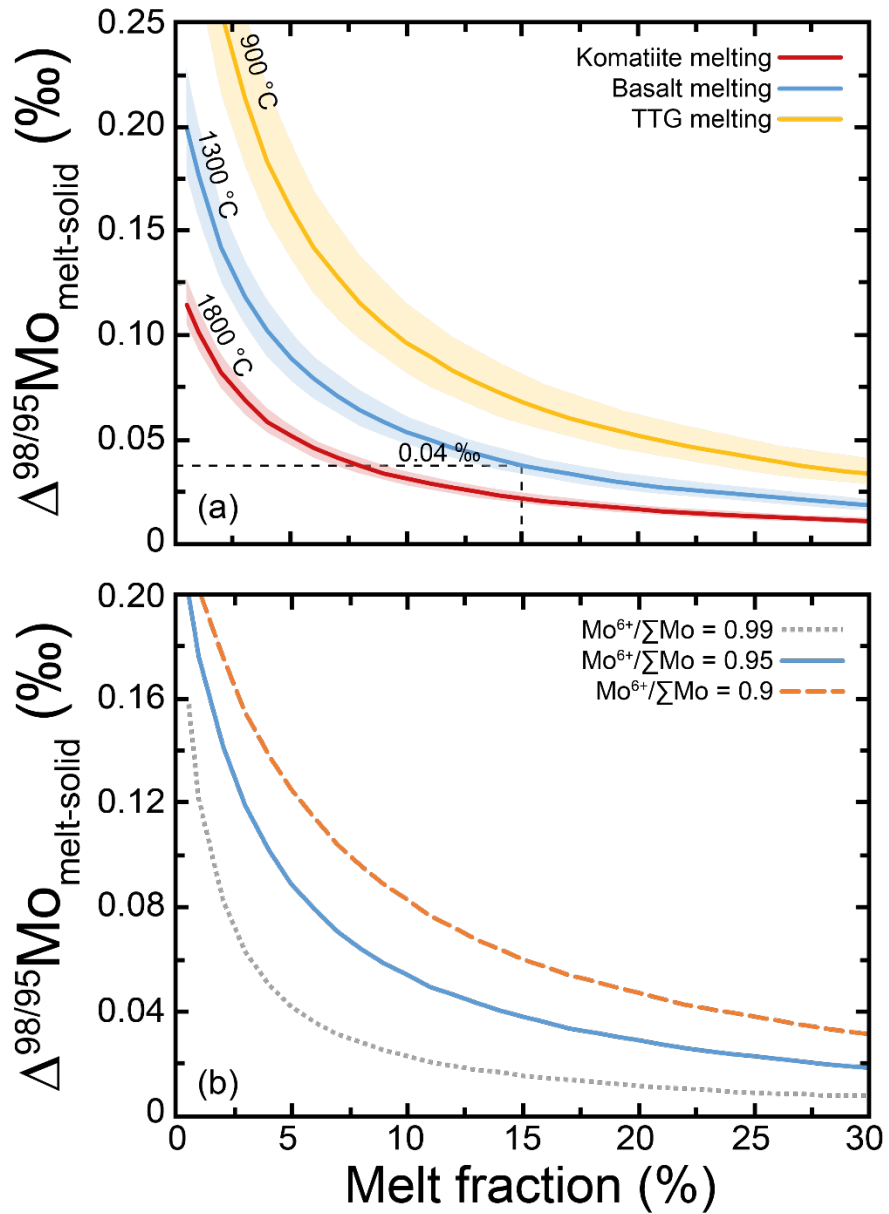
408

409

410

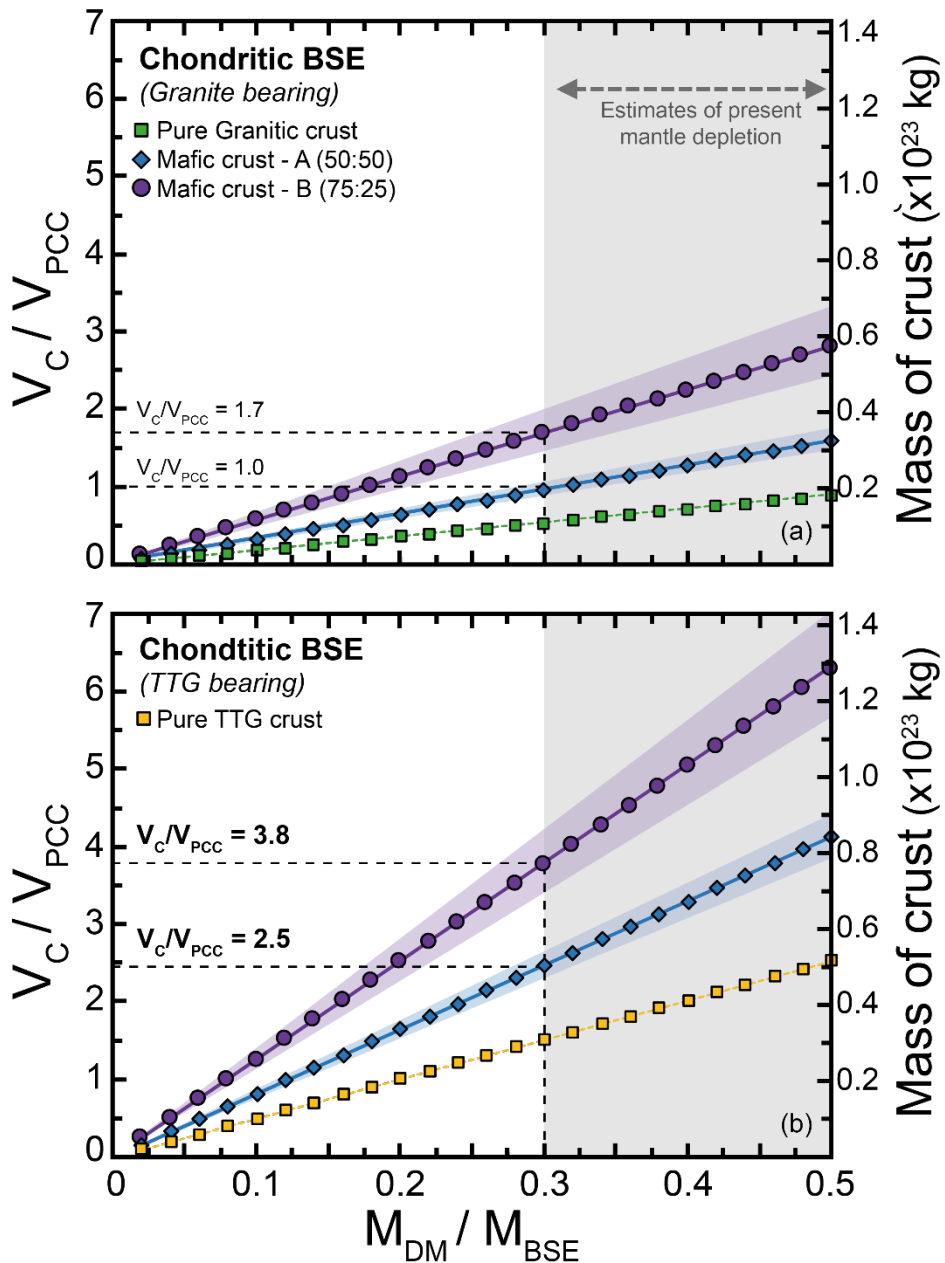
411

Figure 2: Schematic Mo evolution of Earth's mantle and crust during planetary differentiation. Earth accretes from chondritic meteorites thus the bulk Earth initial $\delta^{98}\text{Mo}$ will be chondritic. During core formation 95 % of Earth's Mo is sequestered into the core trapping isotopically light Mo in the metal phase, possibly making the residual BSE heavier. Subsequent extraction of Earth's isotopically heavy crust prior to 3.5 Ga resulted in a bulk mantle that is lighter than the building blocks of Earth. Earth's earliest crust was more mafic than modern crust and therefore had a different Mo concentration and isotopic composition.



412

413 **Figure 3:** Partial melting model showing that the degree of enrichment of heavy Mo isotopes
 414 in the melt phase is controlled by both temperature and the valance state of Mo. (a) the effect
 415 of varying temperature at a constant oxygen fugacity ($\text{Mo}^{6+}/\Sigma\text{Mo} = 0.95$). Shaded areas
 416 represent varying the temperature by ± 100 °C. (b) The effect of varying oxygen fugacity at a
 417 constant temperature (1300 °C).



418

419 **Figure 4:** Results of Mo isotope mass balance calculations which estimate the mass of crust
 420 extraction required to balance the composition of the depleted mantle. This mass of crust can
 421 then be converted into a volume of crust (V_C) relative to the present volume of continental
 422 crust (V_{PCC}) and varies depending on the proportion of the total BSE that has undergone melt
 423 depletion (M_{DM}/M_{BSE}). Mafic crust-A and -B contain mafic and felsic rocks in 50:50 and
 424 75:25 ratios, respectively. The shaded areas represent varying the proportions of the two
 425 endmembers by $\pm 5\%$.

426

427 **Supplementary information for:**
428 **Molybdenum isotope evidence for extensive crustal**
429 **extraction and recycling in Earth's first billion years**

430

431 Alex J. McCoy-West^{1,2}, Priyadarshi Chowdhury², Kevin W. Burton¹, Paolo Sossi³, Geoff M.
432 Nowell¹, J. Godfrey Fitton⁴, Andrew Kerr⁵, Peter A. Cawood² and Helen M. Williams^{1,6}

433

434 ¹Department of Earth Sciences, Durham University, Elvet Hill, Durham DH1 3LE, UK

435 ²School of Earth, Atmosphere and Environment, Monash University, Clayton, Victoria, 3800, Australia

436 ³Institute of Geochemistry and Petrology, ETH Zürich

437 ⁴School of GeoSciences, University of Edinburgh, Edinburgh EH9 3FE, UK

438 ⁵School of Earth and Ocean Sciences, Cardiff University, Park Place, Cardiff CF10 3AT, UK

439 ⁶Department of Earth Sciences, University of Cambridge, Downing Street, Cambridge CB2 3EQ, UK

440

441

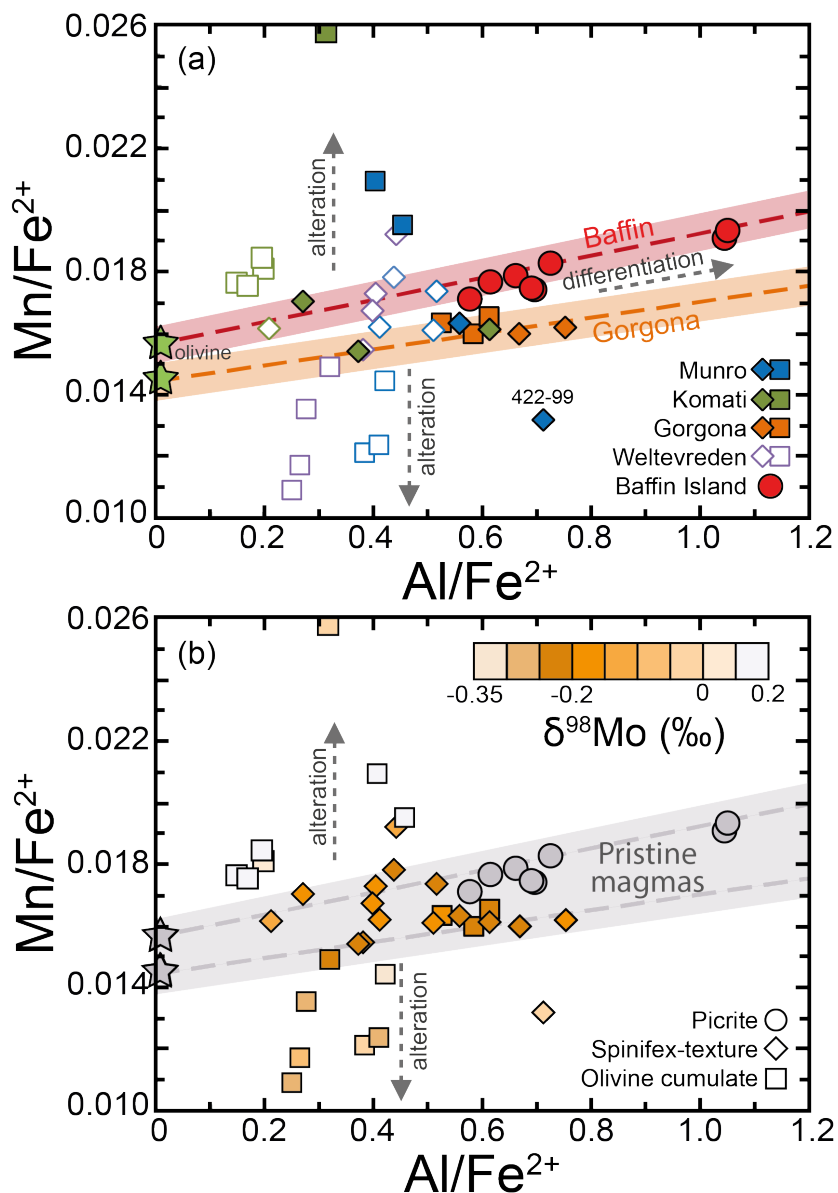
442

443

444 Corresponding author: Alex McCoy-West (alex.mccoywest@monash.edu)

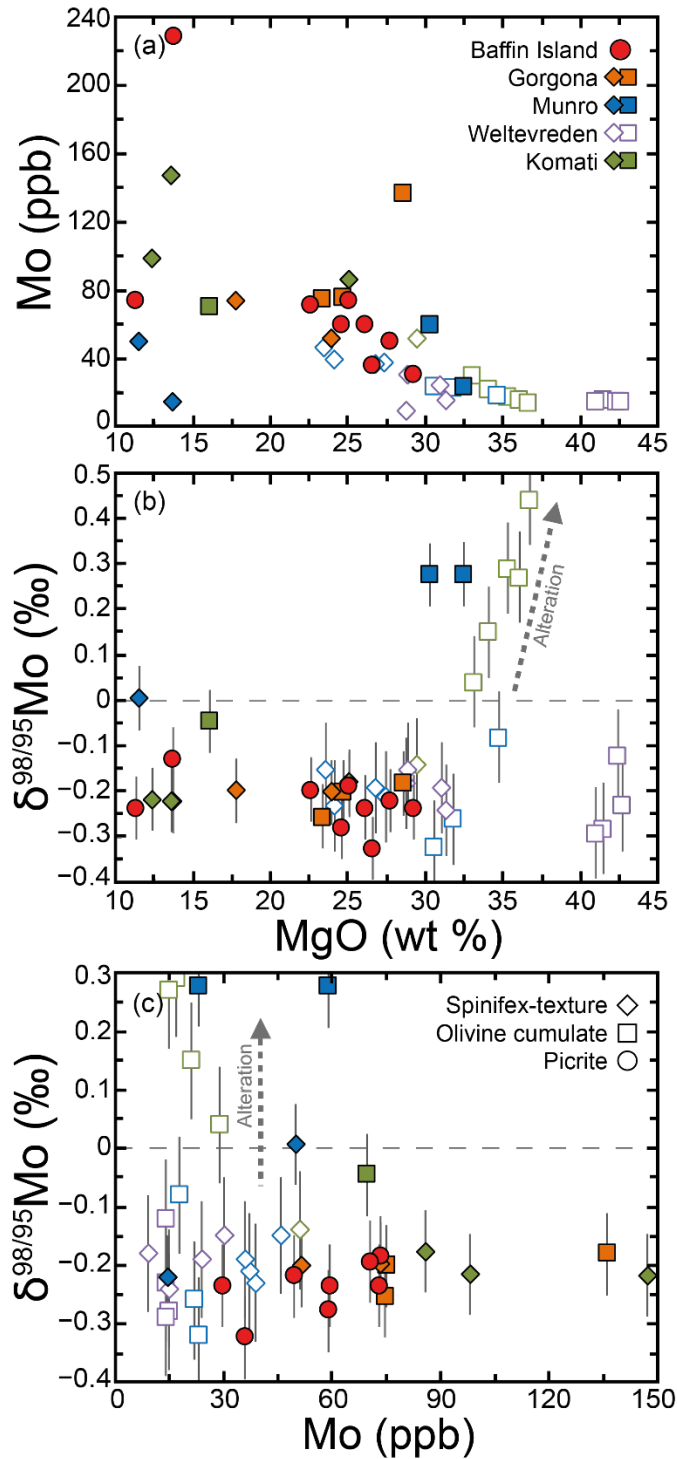
445

Figures and Tables

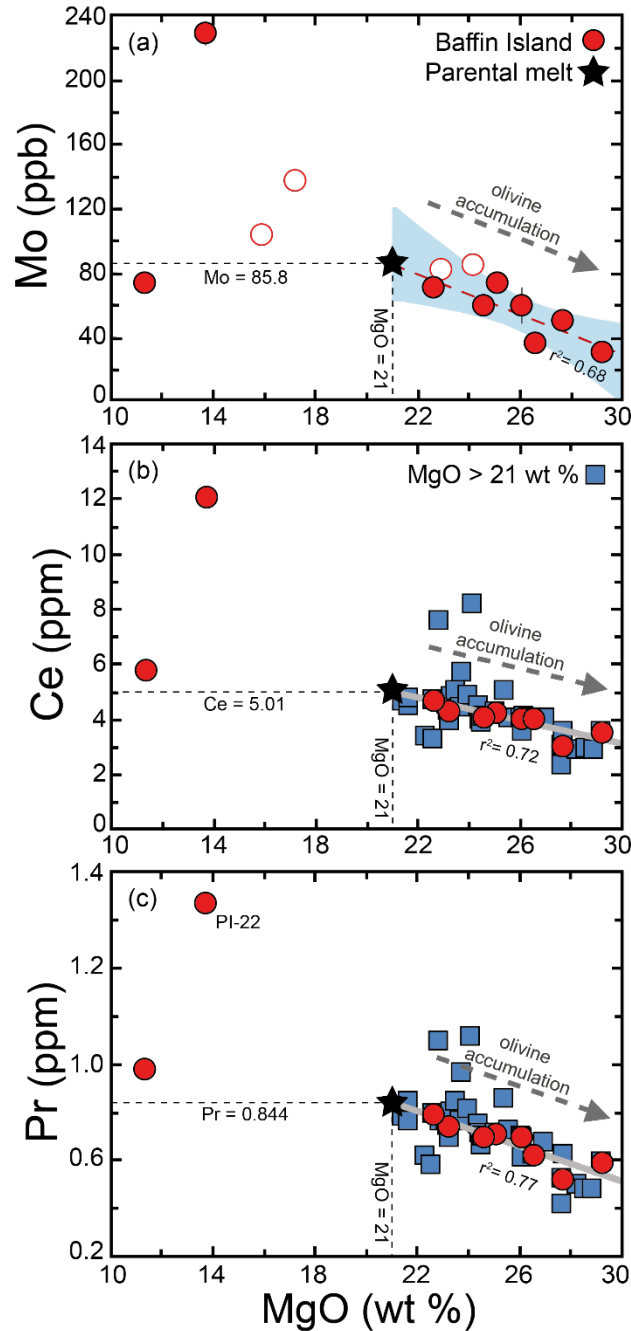


448
449
450
451
452
453
454
455
456
457
458
459
460
461

Supplementary Figure 1: Variation of Mn/Fe²⁺ versus Al/Fe²⁺ in komatiites and picrites. This type of plot is commonly used to assess alteration in komatiites^{1,2}. Different rock types are distinguished: picrites (circles), spinifex textured (diamonds) and olivine cumulates (squares). (A) Filled symbols represent samples analysed herein with hollow symbols samples measured in Greber, et al.^{3,4}. Major element data comes from refs.⁵⁻¹¹. The shaded red and orange fields represent pristine unaltered samples, based on Baffin Island picrites and Gorgona komatiites, with variations the result of accumulation or fractional crystallization of olivine crystals. Samples that fall perpendicular to this trend have experienced elemental mobility and are considered altered. (B) Archean komatiite data is coloured based on the δ⁹⁸Mo of the samples. Gradational scale uses 0.05‰ increments from and -0.35 to 0‰, and 0.1‰ increments above 0‰. All samples with δ⁹⁸Mo ≥ 0.1‰ are plotted with the light grey on the righthand side. Notably, samples with δ⁹⁸Mo between -0.25 and -0.15‰ plot near the unaltered field defined by the Baffin Island and Gorgona magmas.



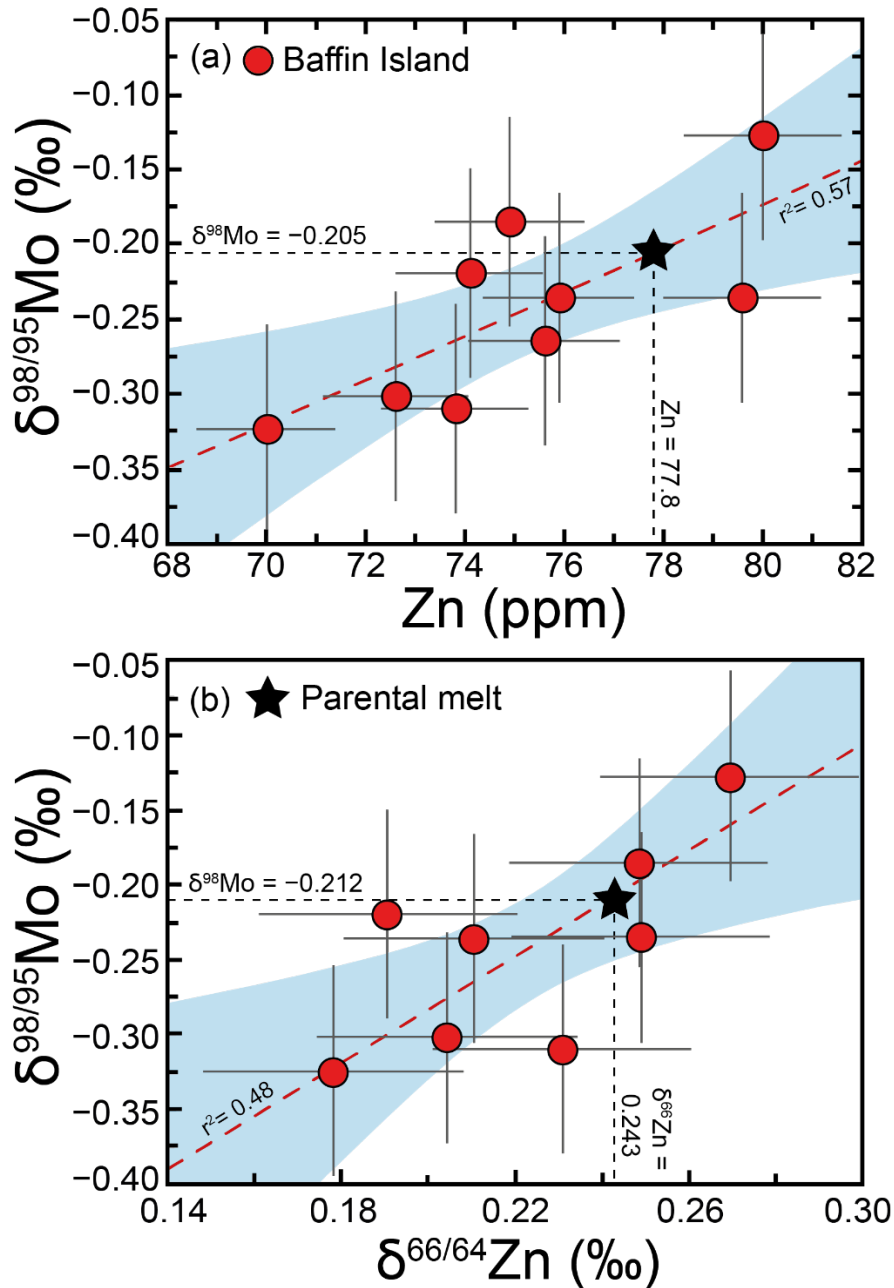
462
 463 **Supplementary Figure 2:** Variation diagrams showing the MgO content, Mo concentration and
 464 $\delta^{98}\text{Mo}$ of komatiites and picrites. Filled symbols represent data analysed herein with hollow symbols
 465 samples investigated in Greber, et al. ³. Error bars on $\delta^{98}\text{Mo}$ are the average reproducibility of the
 466 Baffin Island analyses ($\pm 0.07\text{‰}$). No resolvable covariation is observed between $\delta^{98}\text{Mo}$ and MgO
 467 content. Notably, most spinifex texture lavas produce identical $\delta^{98}\text{Mo}$ within analytical errors at a
 468 wide range of Mo concentration, whereas the olivine cumulates have invariable Mo concentrations
 469 but more variation in $\delta^{98}\text{Mo}$ due to their greater proportion of olivine which is susceptibility to
 470 alteration.



472

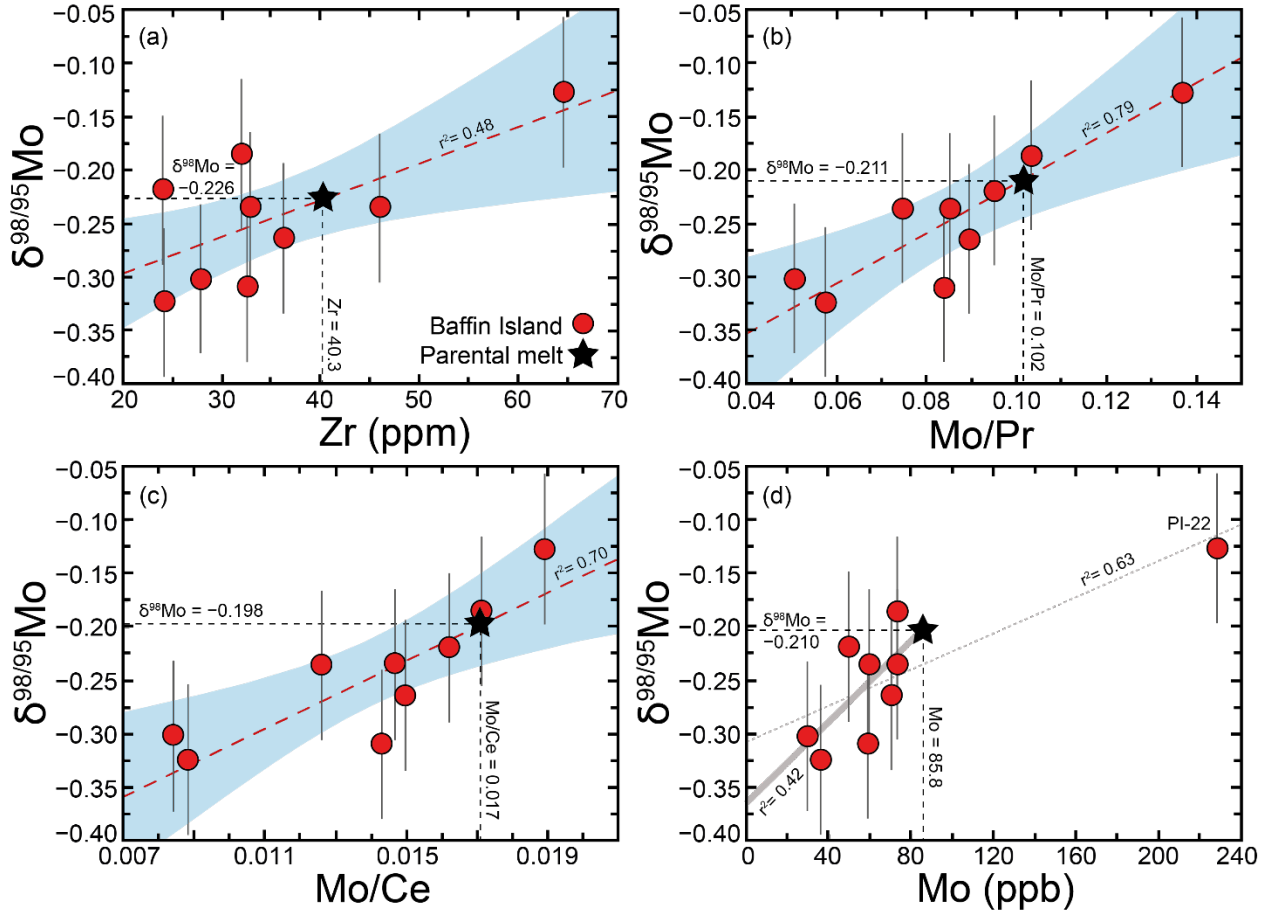
473 **Supplementary Figure 3:** Trace element evidence for olivine accumulation in high-MgO Baffin
 474 Island picrites. Excellent correlations are observed against MgO in samples with >21 wt % MgO. (a)
 475 Variation of Mo concentration versus MgO content. Hollow symbols are samples with only
 476 concentration data. Shaded area represents the 95% confidence interval of the correlation. (b-c) Ce
 477 and Pr concentration, respectively, versus MgO content. Whole rock data comes from Starkey, et al.⁷
 478 with the complete Baffin Island dataset (squares) plotted for comparison. The parental melt (i.e. the
 479 original composition of the magmas from the mantle source region corrected for olivine
 480 accumulation) at Baffin Island was calculated to have 21 wt % MgO (see McCoy-West, et al.¹² for
 481 detailed discussion).

482

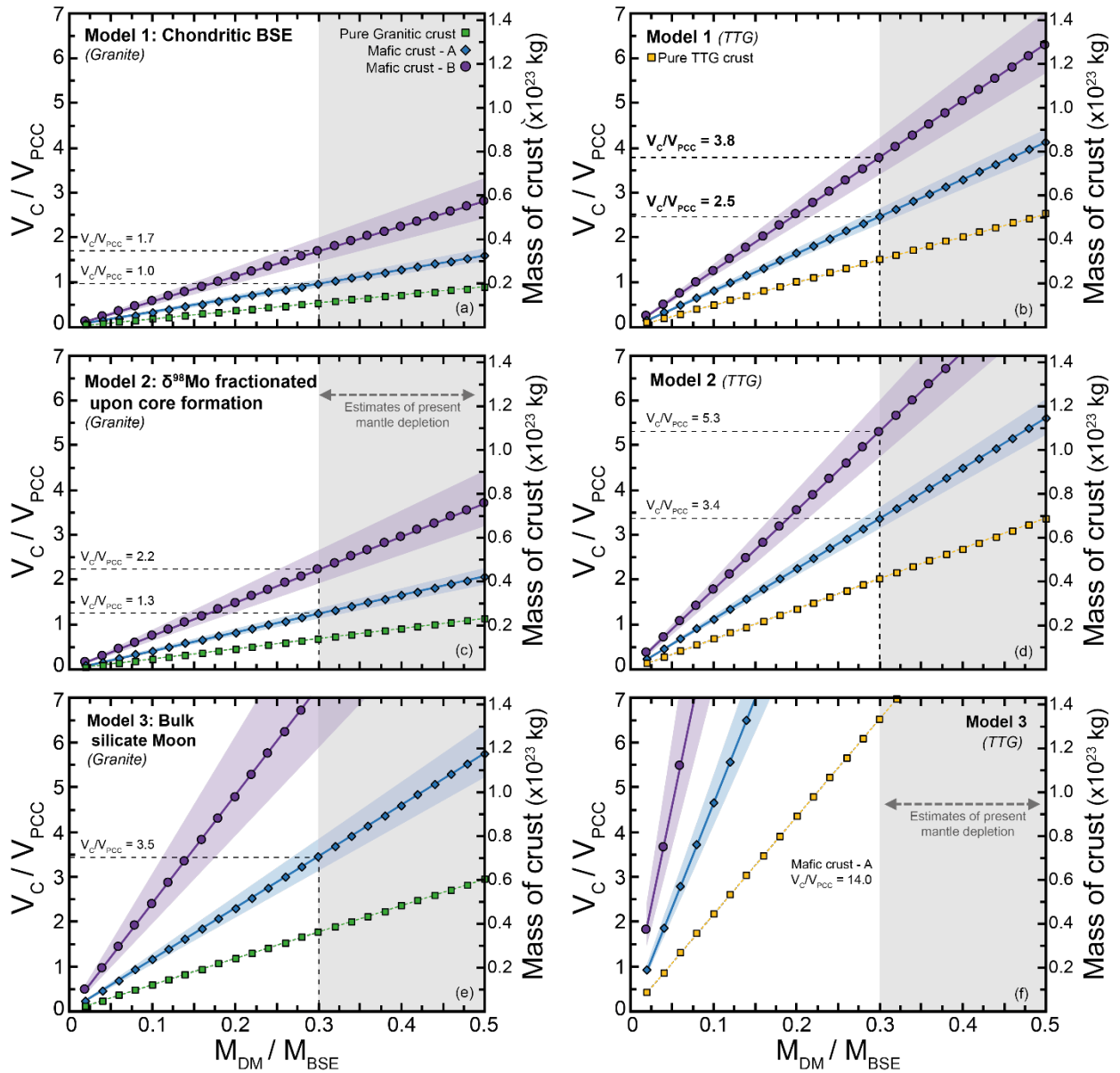


484
 485
 486
 487
 488
 489
 490
 491
 492
 493
 494

Supplementary Figure 4: Variation diagrams of $\delta^{98}\text{Mo}$ versus Zn concentration (a) and $\delta^{66}\text{Zn}$ (b). Comparative Zn data come from Starkey, et al.⁷ and McCoy-West, et al.¹². Shaded area represents the 95% confidence interval of the correlation. Error bars on $\delta^{98}\text{Mo}$ are the average reproducibility of the Baffin Island analyses ($\pm 0.07\text{‰}$), with errors on Zn concentration assumed to be 2% and $\delta^{66}\text{Zn}$ the long-term reproducibility ($\pm 0.03\text{‰}$). The correlation between Zn concentration and $\delta^{66}\text{Zn}$ and the Mo isotope compositions suggests that the variability is controlled by the same process (i.e. olivine accumulation). See McCoy-West, et al.¹² for more detailed discussion of the accumulation of olivine phenocrysts that have experienced kinetic isotope exchange based on Fe and Zn isotopes.



497 **Supplementary Figure 5:** Variation diagrams of $\delta^{98}\text{Mo}$ versus trace element concentrations or
 498 elemental ratios in the Baffin Island picrites. Comparative data come from Starkey, et al. ⁷. Shaded
 499 areas represent the 95% confidence interval on the correlations. Error bars on $\delta^{98}\text{Mo}$ are the average
 500 reproducibility of the analyses ($\pm 0.07\text{‰}$). The strong correlations between MgO content and trace
 501 elements (see Fig. S4) allow calculation of the elemental concentration of the parental melt (i.e. 21 wt
 502 % MgO). This value is then used with the correlations presented above to obtain the $\delta^{98}\text{Mo}$ of the
 503 parental melt (see Table S2). The strong linear trends show this is the result of accumulation (i.e. a
 504 linear addition process) rather than magmatic differentiation (where parabolic curves would be
 505 expected).



508

509

510

511

512

513

514

515

516

517

518

519

520

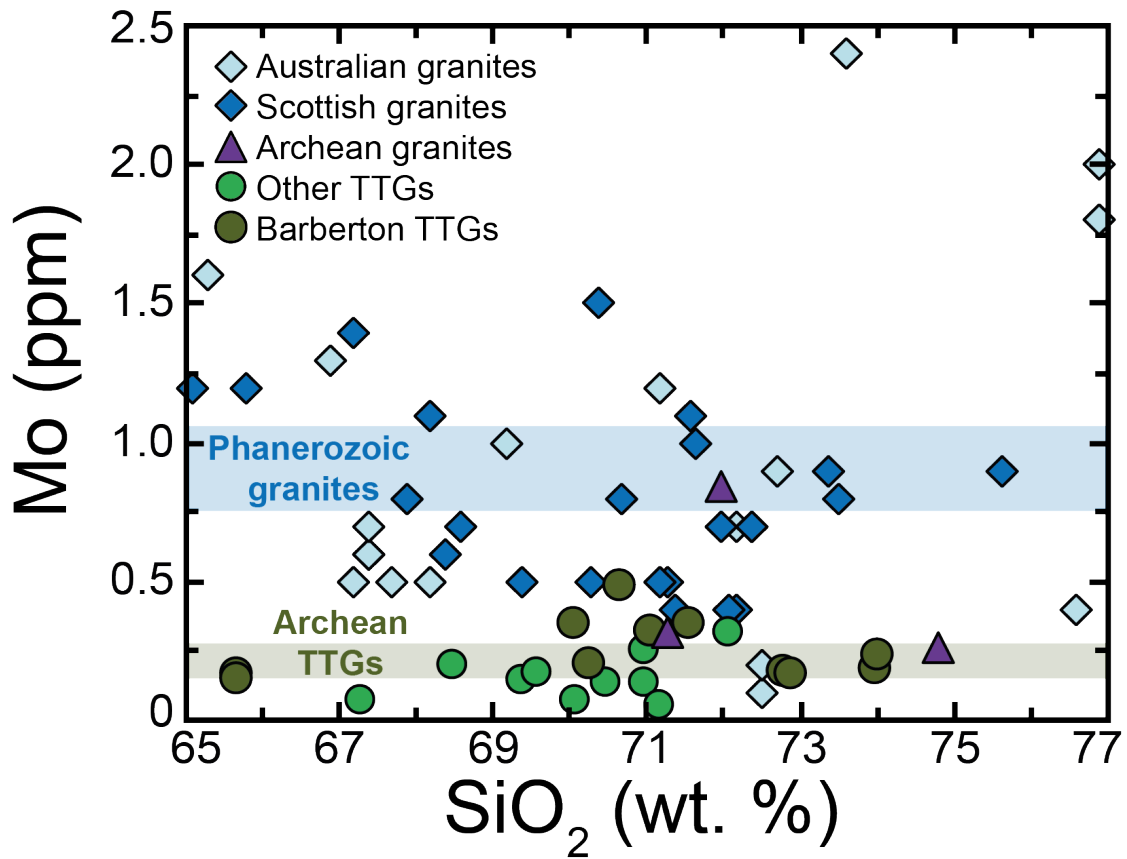
521

522

523

524

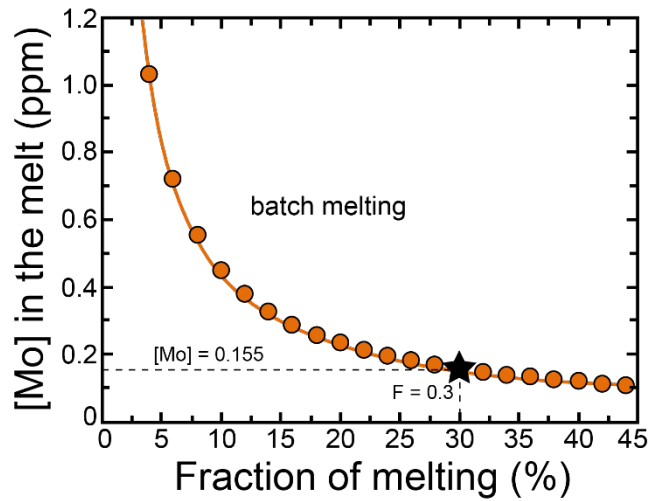
Supplementary Figure 6: Results of Mo isotope mass balance calculations which estimate the mass of crust extraction required to balance the composition of the depleted mantle. This mass of crust can then be converted into a volume of crust (V_C) relative to the present volume of continental crust (V_{PCC}) and varies depending on the proportion of the total BSE that has undergone melt depletion (M_{DM}/M_{BSE}). Thirty-fifty % depletion of the mantle (grey field) can reproduce the radiogenic isotope and incompatible element signatures of the crust and depleted mantle, assuming they represent complementary reservoirs^{10,11,13,14}. (a-b) Model 1: assumes a chondritic BSE for Mo isotopes ($\delta^{98}\text{Mo} = -0.154\%$); (c-d) Model 2: assumes an isotopically heavier BSE following core formation ($\delta^{98}\text{Mo} = -0.142\%$). (e) Model 3: assumes the BSE equilibrate with the composition of the silicate Moon ($\delta^{98}\text{Mo} = -0.078\%$). Crustal volumes are calculated for three different Archean crust types: a purely felsic crust, Mafic crust-A (minimum based on a mafic crust) and Mafic crust-B (a likely Archean crustal composition). Felsic-crust is composed exclusively of felsic rocks, while the Mafic crust-A and -B contain mafic and felsic rocks in 50:50 and 75:25 ratios, respectively. The felsic endmember is either granite (left side: a, c, e) or more realistic for the early Earth has a TTG composition (b, d, f; see Table S5 for further details).



525
 526
 527
 528
 529
 530
 531
 532
 533
 534

Supplementary Figure 7: Comparison of the Mo concentration of Phanerozoic granites and Archean granites and tonalite-trondhjemite-granodiorites (TTGs). Archean samples come from Greaney, et al.¹⁵ and are divided into Barberton TTGs (3.2-3.6 Ga), other TTGs (Zimbabwe and Superior; 2.7-3.0 Ga) and granites (2.6-2.7 Ga). Phanerozoic samples come from Yang, et al.¹⁶, they are divided on the basis of location into Australian (Lachlan and New England orogens; 286-428 Ma) and Scottish (Caledonian plutons; 392-408 Ma) samples. Shaded bars represent the averages for Archean TTGs (Mo = 0.21 ± 0.05 ppm; n = 26;¹⁵) and Phanerozoic granites (Mo = 0.90 ± 0.15 ppm; n = 46;¹⁶).

535



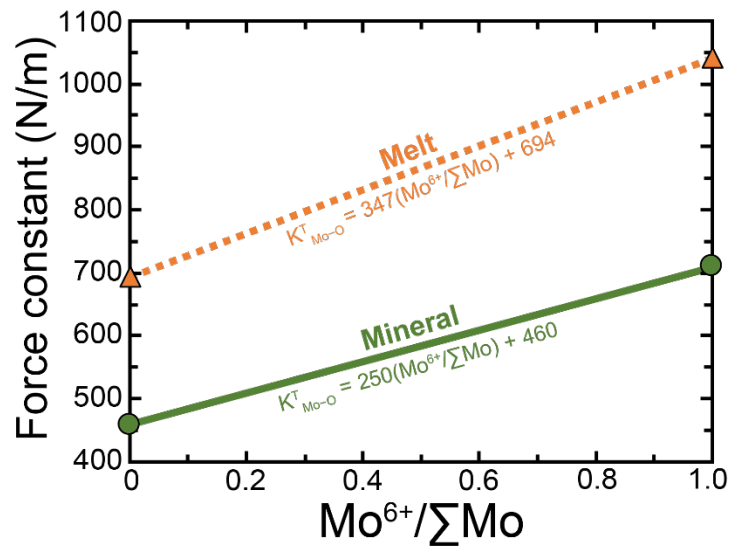
536

537 **Supplementary Figure 8:** Batch melting model show the variation in Mo concentration as a function
538 of melt fraction. Modelling uses a bulk D_{Mo} of 0.006¹⁷ and assumes a source concentration of 0.047
539 ppm¹⁸.

540 The [Mo] of the basalt endmember (0.155) is based on 30% melting of the mantle (sitting in the
541 middle of the Archean range to produce a high Mg basalt;^{19,20})

542

543



544

545 **Supplementary Figure 9:** Force constant of Mo–O bonds in minerals and melt as a function of
546 $\text{Mo}^{6+}/\Sigma\text{Mo}$ used in the modelling presented in Figure 4. Based on values presented in Table S7.

547

548

549

550 **Supplementary Table 1:** Molybdenum concentrations and isotope compositions of high-
 551 degree partial melts and reference materials.

Sample	Location	Rock Type	MgO (wt%)	Mo (ng/g)			$\delta^{98/95}\text{Mo}$			n
				a	b	Average	a	b	Average	
Baffin Island										
PI-22	<i>Padloping Island</i>	pic	13.7	226.0	231.4	229 ±7.6	-0.092	-0.162	-0.127 ±0.098	2
PI-24		pic	26.1	55.6	63.5	59.6 ±11.2	-0.243	-0.227	-0.235 ±0.023	2
PI-25		pic	27.7	49.6	49.3	49.4 ±0.4	-0.181	-0.257*	-0.219 ±0.107	2
PI-26		pic	25.1	74.0	72.7	73.3 ±1.8	-0.169	-0.202*	-0.186 ±0.047	2
PI-28		pic	11.3	75.4	73.0	73.0 ±3.4	-0.244	-0.227*	-0.236 ±0.024	2
PI-31~		pic	22.6	69.8	71.3	70.5 ±2.2	-0.333	-0.195	-0.264 ±0.195	2
PI-37		pic	26.6	35.9	35.6	35.8 ±0.4	-0.305	-0.343*	-0.324 ±0.054	2
PI-40~		pic	29.2	30.0	29.6	29.8 ±0.6	-0.235	-0.369*	-0.302 ±0.189	2
PI-43		pic	24.6	58.5	59.0	58.8 ±0.6	-0.342	-0.278*	-0.310 ±0.090	2
PAD-6^		pic	17.6	137.1	-					
DI-23^	<i>Durban Island</i>	pic	24.1	84.8	-					
DI-26^		pic	15.9	102.9	-					
DUR-8^		pic	22.9	82.1	-					
Gorgona										
GOR94-29	<i>Gorgona Island</i>	STK	17.8	73.3			-0.197	-	-0.197 ±0.070	
GOR94-43		STK	23.9	49.6	53.1	51.4 ±4.9	-0.213	-0.189	-0.201 ±0.034	2
GOR94-3		OC	28.6	135.8			-0.181	-	-0.181 ±0.070	
GOR94-17		OC	23.4	74.6			-0.254	-	-0.254 ±0.070	
GOR94-44		OC	24.7	75.2			-0.201	-	-0.201 ±0.070	
Lower Komati										
331/777a	<i>Komati</i>	STK	25.1	85.7	87.8	86.7 ±3.0	-0.169	-0.184	-0.177 ±0.021	2
331/778		STB	12.3	98.3	-		-0.216	-	-0.216 ±0.070	
331/786		STB	13.6	147.1	-		-0.218	-	-0.218 ±0.070	
331/790#	<i>Mundt's Concession</i>	OC	16.1	69.6	60.3	64.9 ± 13.1	-0.070	-0.020	-0.045 ±0.070	2
Munro										
422/84#	<i>Pyke Hill</i>	OC	30.3	59.1	-		0.276	-	0.276 ±0.070	
422/86#		OC	32.4	23.1	-		0.277	-	0.277 ±0.070	
422/99#		STB	11.5	49.9	-		0.007	-	0.007 ±0.070	
RL-12-1	<i>Red Lake</i>	STB	13.7	14.4	22.2	18.2 ±10.7	-0.242	-0.198	-0.220 ±0.062	2
Mid-ocean ridge basalt										
45N	<i>Mid-Atlantic</i>	E-type		403	418	410 ±21	-0.198	-0.119	-0.159 ±0.056	2
Rock Standards										
AGV-1	<i>Oregon</i>	and	1.5	2186	2062	2101 ±147	-0.154	-0.168		
				2055			-0.169		-0.164 ±0.017	3
BCR-1	<i>Oregon</i>	bas	3.5	1741	1676	1682 ±111	0.066	0.076		
				1630			0.079		0.074 ±0.013	3
BIR-1	<i>Iceland</i>	bas	9.7	32.2	34.1	33.1 ±2.6	-0.111	-0.155	-0.133 ±0.062	2
BHVO-1	<i>Hawaii</i>	bas	7.2	1077	1092	1061 ±85	-0.219	-0.220		
				1025	1103		-0.205	-0.182		
				1006			-0.200		-0.205 ±0.031	5

552 Errors on average Mo concentrations and $\delta^{98/95}\text{Mo}$ are two-standard deviations. For samples with only
 553 one replicate the average reproducibility of the Baffin Island samples is taken as the error ($\pm 0.07\%$;
 554 see the methods section for further discussion). Sample types: pic = picrite; OC = olivine cumulate;
 555 STK = spinifex texture komatiite; STB = spinifex texture basalt; bas = basalt; and =andesite. #
 556 samples are altered and not included in calculating the average composition of Archean komatiites. *
 557 denotes samples that were digested initially using carius tube digestion then followed by HF-HNO₃
 558 digestion. ^ samples that were only run initially for concentrations by isotope dilution. ~ Two samples
 559 did not reproduce very well and the 2 s.d. are large, however, the total range between the replicates is
 560 significantly smaller.

561 **Supplementary Table 2:** Calculation of the Mo isotope composition of the Baffin Island
 562 parental melt

Parameter	Regressions	Value at 21 wt % MgO	$\delta^{98/95}\text{Mo}$ (‰)
Zn (ppm)	Fig. S2 ($r^2 = 0.57$)	77.8	-0.205 ± 0.040
$\delta^{66}\text{Zn}$ (‰)	Fig. S2 ($r^2 = 0.48$)	0.243	-0.212 ± 0.050
Mo/Pr	Fig. 2 ($r^2 = 0.79$)	0.102	-0.211 ± 0.043
Mo/Ce	Fig. S4 ($r^2 = 0.70$)	0.017	-0.198 ± 0.043
Zr (ppm)	Fig. S4 ($r^2 = 0.48$)	40.3	-0.226 ± 0.035
Mo (ppb)	Fig. S4 ($r^2 = 0.42$)	85.8	-0.210 ± 0.068
Average Parental Melt:			-0.210 ± 0.010

563 Errors on $\delta^{98}\text{Mo}$ are calculated from the 95 % confidence interval (error envelopes) on the regressions
 564 calculated using Isoplot²¹ at the composition of the parental melt. The MgO content of the Baffin
 565 Island parental melt was calculated at 21 wt. % MgO using the inflection method (see McCoy-West,
 566 et al.¹²). Given the strong correlations between elemental concentration and MgO content in the
 567 picrites with >21 wt. % MgO, using linear regression concentrations of the elements of interest are
 568 calculated at the parental melt composition. Zn isotope data comes from McCoy-West, et al.¹². Trace
 569 earth element data is from Starkey, et al.⁷.

570

571

572 **Supplementary Table 3:** Locations and Mo isotope compositions of primitive materials used
 573 to calculate the Mo isotope composition of the accessible mantle

Location	$\delta^{98/95}\text{Mo}$ (‰)	2 s.d.	n	References
<i>Depleted-MORB</i>				
Pacific-Antarctic Ridge	-0.206 ± 0.021	± 0.033	5	Bezard, et al. ²²
<i>Phanerozoic picrite</i>				
Baffin Island, NE Canada	-0.210 ± 0.10	± 0.019	6	Herein
<i>Phanerozoic komatiite</i>				
Gorgona, Columbia	-0.207 ± 0.034	± 0.055	5	Herein
<i>Archean komatiites</i>				
Komati, South Africa	-0.187 ± 0.059	± 0.074	4	Herein; Greber, et al. ³
Weltevreden, South Africa	-0.215 ± 0.038	± 0.031	4	Greber, et al. ³
Munro, Canada	-0.196 ± 0.044	± 0.070	5	Greber, et al. ³ ; Herein
<i>Mantle Xenoliths</i>				
Tariat, Mongolia	-0.210 ± 0.093	± 0.177	6	Liang, et al. ²³
Vitim, Siberia	-0.198 ± 0.061	± 0.077	4	Liang, et al. ²³
Accessible Mantle	-0.204 ± 0.008	± 0.018	8	Herein

574 Errors on $\delta^{98}\text{Mo}$ are 95% standard errors (95% s.e. = $t * \text{s.d.}/(n)^{1/2}$, where t = inverse survival
 575 function of the Student's t-test at the 95% significance level and (n-1) degrees of freedom), with two-
 576 standard deviation (2 s.d.) also shown to represent population uncertainty. Depleted mid ocean ridge
 577 basalts (MORB) are only those samples with measured $^{143}\text{Nd}/^{144}\text{Nd} \geq 0.513117$. Mantle xenoliths
 578 from Kilbourne Hole, New Mexico were excluded due to their large spread in $\delta^{98}\text{Mo}$ values (0.32 ‰)
 579 and limited sample set (n = 3).

580

581

582 **Supplementary Table 4:** Molybdenum isotope compositions of geochemical reservoirs
 583 presented in Figure 1 or used in modelling

Reservoir	$\delta^{98/95}\text{Mo}$ (‰)	2 s.d.	n	References
-----------	-------------------------------	--------	---	------------

Chondrites	-0.154 ±0.013	±0.051	18	Liang, et al. ²³ , Burkhardt, et al. ²⁴
Archean komatiites	-0.199 ±0.019	±0.062	13	Herein
Mantle peridotites	-0.206 ±0.050	±0.180	15	Liang, et al. ²³
Global basalts	-0.10 ±0.04	±0.27	57	Yang, et al. ¹⁶ and therein
Global granites	0.16 ±0.05	±0.41	55	Yang, et al. ¹⁶ and therein
Upper Continental Crust	0.14 ±0.07		112	Yang, et al. ¹⁶

584 Errors on $\delta^{98}\text{Mo}$ are 95% standard errors (95% s.e. = $t * \text{s.d.}/(n)^{1/2}$, where t = inverse survival
585 function of the Student's t-test at the 95% significance level and $(n-1)$ degrees of freedom), with two-
586 standard deviation (2 s.d.) also shown to represent population uncertainty. Chondrite average
587 excludes CK and CM groups meteorites. Upper continental crust composition was calculated
588 assuming a 10:1 proportion of felsic to basaltic rocks ¹⁶.

589

590

591

592

593 **Supplementary Table 5:** Molybdenum concentration and isotopes compositions of
 594 geochemical reservoirs used in mass balance calculations

Reservoir	Mass (kg) ^a	Density (kg/m ³)	Mo (ppm)	$\delta^{98/95}\text{Mo}$ (‰)
Chondrites			ca. 1.7 ^b	-0.154 ± 0.013 ^{f,g}
Earth	5.9376 x 10 ²⁴			
Core	1.932 x 10 ²⁴		ca. 5 ^b	-0.16 ± 0.02 ^f
Bulk silicate Earth	4.0603 x 10 ²⁴		0.047 ± 0.019 ^c	-0.154
Mantle	4.0343 x 10 ²⁴			
Depleted mantle	Varied		0.025 ± 0.007 ^d	-0.204 ± 0.008
Modern crust	2.6 x 10 ²²			
Mafic endmember		3000	0.155	-0.10 ± 0.04 ^h
Types of Crust				
<i>Granite bearing models</i>				
Pure Granitic crust		2750	0.47 ^d	0.16 ± 0.07 ^h
Mafic crust A (50:50)		2850 ± 15	0.313 ± 0.016	0.096 ± 0.010
Mafic crust B (75:25)		2925 ± 15	0.234 ± 0.016	0.031 ± 0.018
<i>TTG bearing models</i>				
Pure TTG crust		2750	0.28 ^d	0.03
Mafic crust A (50:50)		2850 ± 15	0.218 ± 0.006	-0.016 ± 0.006
Mafic crust B (75:25)		2925 ± 15	0.186 ± 0.006	-0.051 ± 0.008

595 Mafic crust compositions were calculated by mixing different proportions of mafic and felsic material
 596 (i.e. 75:25 is 75% mafic). Molybdenum concentration data shows that Phanerozoic granites are clearly
 597 more evolved than their Archean counterparts (see Fig. S7). The Mo concentration of the felsic
 598 endmembers were taken from the available published data in Greaney, et al. ¹⁵, using the average
 599 composition of the oldest 3.5 Ga Barberton TTGs (0.28; n = 15), and 2.7 Ga granites (0.47; n = 3)
 600 available. The Mo concentration of the mafic endmember (Mo = 0.155) was calculated based on batch
 601 melting of the bulk silicate Earth assuming an F of 0.3 (higher than today due to the elevated mantle
 602 temperatures in the Eoarchean) and a bulk D_{Mo} of 0.006 ¹⁷ (see Fig. S8). The isotopic composition of
 603 mafic endmember uses the modern global basalt average of $\delta^{98}\text{Mo} = -0.10 \pm 0.04$ ‰ (n = 57). Partial
 604 melting is a time invariant process at constant temperature and therefore the modern basalts provide a
 605 good analogue. The partial melting model presented in Figure 4 shows that a melt will 0.05‰ heavier
 606 than its mantle source (chondrite BSE) as required in this instance from 12-15 % melting. The
 607 formation of TTGs requires the remelting of metabasalt, given that TTGs have lower Mo
 608 concentrations than granites it is sensible to assume their $\delta^{98}\text{Mo}$ will also be less evolved. Here we
 609 have taken the simplest approach (i.e. two step formation of TTGs) and taken the average of global
 610 basalts and granites to estimate the $\delta^{98}\text{Mo}$ of TTG felsic component. Densities were calculated by
 611 mixing basaltic (3000 kg/m³) and granitic (2700 kg/m³) endmembers. Errors on Mafic crusts (A and
 612 B) represent varying the proportions of the two endmembers by 5%. References for other parameters
 613 as follows: a) Yoder ²⁵; b) McDonough ²⁶; c) Palme and O'Neill ¹⁸; d) Salters and Stracke ²⁷; e)
 614 Rudnick and Gao ²⁸; f) Burkhardt, et al. ²⁴; g) Liang, et al. ²³; h) Yang, et al. ¹⁶.

615

616 **Supplementary Table 6:** Model parameters for the calculation of Mo isotope fractionation
 617 during non-modal batch melting

Phase	Starting fraction*	Melting reaction*	$D_{\text{Mo}4+}^{\wedge}$	$D_{\text{Mo}6+}^{\wedge}$
Olivine	0.6	-0.15	0.5	0.006

Orthopyroxene	0.25	0.15	0.7	0.009
Clinopyroxene	0.1	1.0	0.3	0.001

618 *Melting parameters come from Walter²⁹. ^ Partition coefficients are taken from Leitzke, et al.³⁰.
619 Model assumes that the force constant is a linear function of $\text{Mo}^{6+}/\sum\text{Mo}$ for both minerals and melt
620 and that all minerals have the same $\text{Mo}^{6+}/\sum\text{Mo}$. Modelling uses force constants calculated in Table
621 S7.

622

623 **Supplementary Table 7:** Parameters used for the calculation of force constants of Mo
624 isotopes in minerals and melts at varied oxidation state.

	\bar{Z}_{Mo}	$C_{\text{N Mo}}$	\bar{S}_{Mo}	\bar{S}_{O}	$r_{\text{Mo-O}}$ (m)	$K_{f\text{Mo-O}}$ (N/m)	$K^{\text{T}}_{\text{Mo-O}}$ (N/m)
<i>Melt</i>							
$\text{Mo}^{6+}\text{O}_4(2-)$	6	4	1.5	0.5	1.76^{-10}	349.8	1040.8
$\text{Mo}^{4+}\text{O}_4(4-)$	4	4	1.0	0.5	1.76^{-10}	233.2	693.9
<i>Minerals</i>							
Mo^{6+}O_3	6	6	1.0	0.5	2.00^{-10}	158.9	709.3
Mo^{4+}O_2	4	6	0.67	0.5	2.02^{-10}	102.8	459.0

625 \bar{Z}_{Mo} = cation charge; C_{N} = coordination number. \bar{S}_{Mo} and \bar{S}_{O} is the average bond valence of
626 molybdenum and oxygen, respectively. $r_{\text{Mo-O}}$ = Bond length in meters. $K_{f\text{Mo-O}}$ = is the force constant
627 approximated by solving the Born-Lande equation. $K^{\text{T}}_{\text{Mo-O}}$ = is the total force constant corrected by a
628 scaling factor related to the proportion of ionic bonds (the ionicity of the Mo–O bond based on the
629 Pauling scale is 0.336). All formulas required for calculating force constants can be found in Sossi
630 and O'Neill³¹. Molybdenum is VI-fold (octahedral) co-ordinated in minerals^{32,33} and predominantly
631 IV-fold (tetrahedral) in silicate melts³⁴. The main uncertainty comes from the bond length of Mo in
632 mineral phases (e.g. olivine, pyroxene), here we use the values for pure Mo oxides taken from Farges,
633 et al.³⁴. Given that Mo is a trace element it should have a similar bond length to Mg and Fe in olivine
634 (2.05^{-10} m), which is comparable to that of the pure metals. Farges, et al.³⁴ also present the Mo–O
635 bond length of sodium silicates melts which provides the best estimate of this parameter in basaltic
636 melts.

637

638 **Supplementary Table 8:** Leaching experiments on Baffin Island picrites.

Sample	Whole Rock		Residue (Silicates)		Leachate (Non-silicates)	
	Mo (ng/g)	$\delta^{98/95}\text{Mo}$	Mo (ng)	$\delta^{98/95}\text{Mo}$	Mo (ng)	$\delta^{98/95}\text{Mo}$
PI-37	35.8	-0.324 ± 0.054	~11	-0.323 ± 0.054	~7	-0.403 ± 0.051
PI-43	58.8	-0.310 ± 0.090	~16	-0.263 ± 0.026	~10	-0.374 ± 0.034

639 A second aliquot of the same sample powder was sealed in a carius tube with 9 mL of reverse Aqua
640 Regia (4:5 HCl-HNO3) and heated to 220°C for >72 hours. Following cooling the Aqua Regia
641 supernatant was removed (henceforth the leachate; predominantly chromite and any sulfides present)
642 and the remaining residual material (henceforth the residue; predominantly silicates) were spiked and
643 processed separately through chemistry.

644 **Methods**

645 *Molybdenum separation*

646 All chemical separations were undertaken within the Arthur Holmes Isotope
647 Geochemistry Laboratories at Durham University. The samples analysed herein have
648 previously been extensively characterised Baffin Island^{12,35} and Archaean Komatiites
649^{8,36} with all powders created in Agate mills. Between 0.1-1.1 g of whole rock powder
650 was weighed out to obtain ca. 30-150 ng of natural Mo and spiked with an equal
651 amount of a ⁹⁷Mo–¹⁰⁰Mo double-spike to yield the ideal spike sample ratio of 1:1³⁷.
652 Two digestion methods were implemented in this study: 1) Most samples were
653 digested in 15 mL Savillex beakers containing a 3:1 mixture of 29M HF + 16M HNO₃
654 on a hotplate at 130°C for ≥72 hours. Following evaporation, the samples were
655 refluxed several times in 16M HNO₃ and 6M HCl to ensure complete decomposition
656 of fluorides. For any samples that contained visible chromite or spinel grains the
657 dissolved silicate portion was removed and saved, and an additional Parr bomb
658 digestion step was undertaken to completely dissolve any refractory minerals. 2)
659 Alternatively, carius tubes digestions were undertaken on some Baffin Island samples
660 whereby ~1.0 g of sample powder was double spiked and mixed with 9 mL of reverse
661 Aqua Regia (4:5 HCl-HNO₃), the tubes were subsequently sealed and heated to 220°C
662 for >72 hours. Following cooling the carius tubes were opened and the supernatant
663 and all undissolved silicate material was removed, using multiple rinses with MQ
664 H₂O. This material was then further processed with a conventional HF-HNO₃ hotplate
665 digestion, to dissolve the refractory silicate portion.

666 A leaching experiment was undertaken on two of the Baffin Island picrites (PI-37, PI-
667 43). A second aliquot of the same sample powder was sealed in a carius tube with 9 mL of
668 reverse Aqua Regia (4:5 HCl-HNO₃) and heated to 220°C for >72 hours. Following cooling

669 the Aqua Regia supernatant was removed (henceforth the leachate; predominantly chromite
670 and any sulfides present) and the remaining residual material (henceforth the residue;
671 predominantly silicates) was then rinsed three times with MQ H₂O. The residue was then
672 dried for reweighing and subsequently digested using conventional HF-HNO₃ digestion as
673 described above. When fully dissolved the concentration of Mo in the two splits was
674 obtained and the samples were spiked using the ⁹⁷Mo–¹⁰⁰Mo double spike and then refluxed
675 several times in concentrated HNO₃ to equilibrate the spike and sample.

676 Chemical separation of Mo was achieved using anion exchange (AG1-x8)
677 chromatography following the procedure described by Willbold, et al. ³⁸. The samples are
678 loaded onto the columns in 5 mL of 3M HCl + 0.05M ascorbic acid, the addition of ascorbic
679 acid converts Fe³⁺ to Fe²⁺ which aids in elution of Fe from the anion exchange resin. This
680 reaction is accompanied by a colour change from yellow to colourless when the reaction has
681 been complete. Prior to loading all sample solutions were transferred into 15 mL centrifuge
682 vials and centrifuged to remove any precipitates that may have formed in the dilute HCl
683 loading solution. The sample matrix is then eluted in 3 mL of 3M HCl, 13 mL of 0.5M HCl
684 + 0.5% H₂O₂, 10 mL of 1M HF and 3 mL of MQ H₂O, prior to collection of the purified Mo
685 fraction in 12 mL of 1M HCl. Larger samples with >0.5g of material were loaded onto the
686 columns in 10-15 mL of 3M HCl to ensure complete dissolution of the samples. These high
687 mass samples were also processed through the complete chemical separation procedure twice
688 to ensure the complete removal of Fe and Ru that can provide isobaric interferences during
689 mass spectrometry. Total Mo procedural blanks calculated following double-spike
690 deconvolution range from 0.18 to 0.40 ng (n = 7) and are considered negligible.

691 *Mass Spectrometry*

692 Molybdenum isotope compositions were measured using a Thermo-Finnigan Neptune multi-
693 collector induction coupled plasma mass spectrometers (MC-ICP-MS). Samples were

694 introduced using an Aridus II desolvating nebuliser and a low uptake rate Cetac35 nebuliser
695 (aspiration rate 25-35 μmin^{-1}). All measurements were made in low resolution using X-
696 cones, and static collection mode with the simultaneous measurement of 9 isotopes ^{91}Zr ,
697 ^{92}Mo , ^{94}Mo , ^{95}Mo , ^{96}Mo , ^{97}Mo , ^{98}Mo , ^{99}Ru and ^{100}Mo . Standard operation involved
698 introduction of 150 ppb Mo double-spiked solutions in 0.5M HNO_3 with trace HF and
699 produced a maximum sensitivity was $\sim 380 \text{ Vppm}^{-1}$. Each analysis consisted of 1 block of
700 50 cycles with a 4 s integration time and was immediately preceded by the analysis of an acid
701 blank, with a washout of 180 s occurring after each sample. Due to the low aspiration rate a
702 single analysis used $<200 \mu\text{l}$ of solution. All Mo isotope measurements herein are reported
703 relative to the internationally accepted reference solution the National Institute of Standards
704 and Technology (NIST) SRM3134^{39,40} where $\delta^{98}\text{Mo} = 0\text{‰}$ as convention dictates. In all
705 cases, conventional delta (δ) notation is used to express the ratios:

$$706 \quad \delta^{98/95}\text{Mo} = [((^{98}\text{Mo}/^{95}\text{Mo})_{\text{SAMPLE}} / (^{98}\text{Mo}/^{95}\text{Mo})_{\text{NIST 3134}}) - 1] \times 1000 \quad (1)$$

707 Data reduction was carried out using the Isospike plugin⁴¹ for Iolite⁴² which is underpinned
708 by the double spike deconvolution equations of Rudge, et al.³⁷. Baseline subtraction was
709 undertaken using the 60 s of acid blank that immediately preceded a sample, with direct
710 isobaric interferences from Zr on ^{92}Mo , ^{94}Mo and ^{96}Mo and Ru on ^{96}Mo , ^{98}Mo and ^{100}Mo
711 mass fractionation corrected iteratively using the beta-factors calculated following the initial
712 deconvolution. In addition to using the double spike to correct for instrumental mass
713 fractionation, a secondary correction for within run mass spectrometer drift was applied using
714 IsoSpike. The Mo isotope compositions of the unknowns were corrected using linear
715 interpolation by adjusting the composition of the bracketing analyses of the primary standard
716 NIST3134, run at least every two unknowns, to 0‰.

717 The long-term stability of the mass spectrometer over a two-year period was
718 confirmed by repeated measurement of the in-house standard Romil which has an average

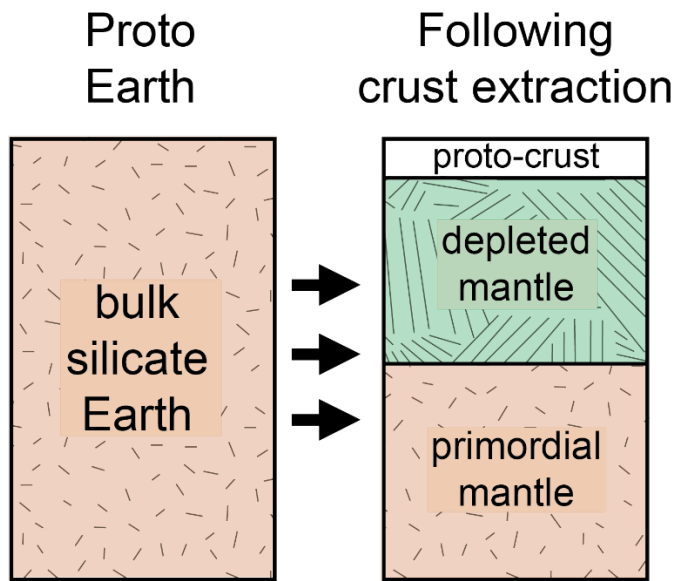
719 $\delta^{98}\text{Mo}$ of $0.045 \pm 0.027\text{‰}$ (2 s.d.; $n = 327$). Long-term accuracy was tested by repeated
720 analyses of international standard solutions Open University ($-0.341 \pm 0.032\text{‰}$, $n = 58$) and
721 Bern ($-0.242 \pm 0.029\text{‰}$, $n = 73$), which are within error of previous determinations^{40,43}. The
722 reproducibility of analyses was further evaluated using a range of US Geological Survey rock
723 standards. A range of first generation rock standards (BCR-1, BHVO-1, and AGV-1) were
724 analysed here (see Table 1), multiple digestions ($n = 3-5$) reproduce to better than 0.031‰ ,
725 however, both BCR-1 and BHVO-1 have lower Mo concentrations and distinctly different
726 $\delta^{98}\text{Mo}$ than their second generation counterparts (i.e. BHVO-2)^{24,44,45}, which suggests that
727 these samples were contaminated with Mo during preparation of the second aliquot as
728 suggested previously^{38,46}. Two separate digestions of low Mo (~ 30 ng/g) standard BIR-1
729 yield an average $\delta^{98}\text{Mo}$ of $-0.133 \pm 0.062\text{‰}$, which is within error of the previous estimate³⁸.
730 Replicate digestions of the high mass, low Mo (30-75 ng/g) Baffin Island and komatiite
731 samples herein generally reproduce to better than $\pm 0.10\text{‰}$, with two samples having
732 significantly larger 2 s.d. (the statistics are poor with only two replicates) although their total
733 range in $\delta^{98}\text{Mo}$ is $<0.14\text{‰}$. Therefore, we conservatively consider $\pm 0.07\text{‰}$ as the long-term
734 reproducibility of the measurements herein (the average 2 s.d. variability on the replicates
735 herein is $\pm 0.068\text{‰}$; $n = 14$).

736

737

738 **Mass balance calculations**

739 The distribution of $\delta^{98}\text{Mo}$ between the depleted mantle and crust after differentiation can be
 740 estimated using isotopic and elemental mass balance (e.g. Willbold and Elliott ⁴⁶). The
 741 equations presented here are similar to those used previously in Hofmann ⁴⁷. Here we
 742 consider that Mo of a portion of the *bulk silicate Earth* (BSE) has been accessed for crust
 743 formation and is distributed among two reservoirs; a *depleted mantle* (DM) and a *proto-crust*
 744 (C) (see Fig. S10). Previous studies using radiogenic isotopes suggest that only 30-50 % of
 745 whole mantle has been depleted ^{10,11,13,14}, which suggests that the mass of mantle sampled is
 746 less than that of whole BSE, i.e. $m_{DM} \ll m_{BSE}$, and $m_{DM} = m_{BSE}$ only if the whole BSE mass
 747 has been used for crust extraction, which is probably not the case ^{10,11,13,14}.



Supplementary Figure 10: During crust formation a portion of the bulk silicate Earth (BSE) is tapped and distributed among two reservoirs; a depleted mantle (DM) and a proto-crust (C). Given that only 30-50 % of whole mantle has been depleted to form the crust: $m_{DM} + m_C \ll m_{BSE}$, meaning a primordial mantle reservoir remains untapped.

748
 749 The isotopic mass balance can be written as follows:

750
$$m_{BSE}[\text{Mo}]_{BSE} \delta_{BSE}^{98/95} = m_C[\text{Mo}]_C \delta_C^{98/95} + m_{DM}[\text{Mo}]_{DM} \delta_{DM}^{98/95} \quad (\text{A})$$

751 Where m is the mass, $[\text{Mo}]$ is the Mo concentration, and $\delta^{98/95}$ is the Mo isotope
 752 composition (i.e. $\delta^{98}\text{Mo}$) of the various reservoirs (BSE, DM and C).

753 The pure elemental mass balance is:

754
$$m_{BSE}[\text{Mo}]_{BSE} = m_C[\text{Mo}]_C + m_{DM}[\text{Mo}]_{DM} \quad (\text{B})$$

755 where, the terms denote similar meanings as above.

756 Substituting for “ $m_{AM}[Mo]_{BSE}$ ” in Eq. A by Eq. B, we have:

$$m_C[Mo]_C \delta_C^{98/95} = (m_C[Mo]_C + m_{DM}[Mo]_{DM}) \delta_{BSE}^{98/95} - m_{DM}[Mo]_{DM} \delta_{DM}^{98/95}$$

$$m_C[Mo]_C (\delta_C^{98/95} - \delta_{BSE}^{98/95}) = m_{DM}[Mo]_{DM} (\delta_{BSE}^{98/95} - \delta_{DM}^{98/95})$$

757
$$m_C = \frac{m_{DM} \cdot [Mo]_{DM} \cdot (\delta_{BSE}^{98/95} - \delta_{DM}^{98/95})}{[Mo]_C \cdot (\delta_C^{98/95} - \delta_{BSE}^{98/95})} \quad (C)$$

758 This allows us to calculate the mass of crust generated assuming various amounts of
759 depletion of the mantle reservoir (see Fig. 4).

760 The volume of this crust can then be calculated using the following:

761
$$V_{crust} = m_{crust} / \rho_{crust} \quad (D)$$

762 where, V_c & ρ_c represent the volume and average density of the crust.

763 This volume is then easily comparable to the present volume of continental crust (PVCC)
764 which is assumed to be $7.2 \times 10^9 \text{ km}^3$ ⁴⁸. The parameters used in mass balance calculations
765 herein are presented in Table S5. Here we have investigated two scenarios to encompass the
766 variability of $\delta^{98}\text{Mo}$ and $[Mo]$ in Archean felsic rocks (granites or TTGs represent the felsic
767 endmember; Fig. 4). Crustal volumes are then calculated for three different model Archean
768 proto-crusts: a hypothetical purely felsic crust, Mafic crust-A (minimum based on a mafic
769 crust) and Mafic crust-B (a likely Eoarchean crustal composition). The felsic crust TTG-crust
770 is composed exclusively of granite or TTG rocks, while the Mafic crust-A and -B contain
771 mafic rocks and TTGs felsic rocks in 50:50 and 75:25 proportions, respectively. Given the
772 dominance of mafic lithologies within the Earth’s early crust >3 Ga^{49,50} it is reasonable to
773 assume that the crust extracted prior to 3.5 Ga was more mafic than today.

774 **Supplementary Text**

775 *Filtering for alteration and the composition of Archean komatiites*

776 Due to their long residence in the crust the $\delta^{98}\text{Mo}$ of komatiites may have been modified by
777 alteration or metamorphism due to the mobility of Mo in fluids^{51,52}. Here we have used a
778 plot of Mn/Fe^{2+} versus Al/Fe^{2+} to assess the extent of alteration in the komatiites (Fig. S1).
779 This type of plot has been used previously to assess alteration in komatiites^{1,2}. Given that Fe
780 and Mn have similar chemical behaviour during magmatic differentiation; olivine generally
781 has a similar Mn/Fe^{2+} as the initial melt, therefore addition or crystallisation of olivine will
782 not significantly fractionate Mn/Fe^{2+} . Therefore, samples that plot perpendicular to the
783 magmatic differentiation trend must have been affected by Fe or Mn mobilization and their
784 $\delta^{98}\text{Mo}$ values may have been modified by secondary alteration after emplacement. For the
785 data presented previously by Greber, et al.³ the olivine-cumulates from the Weltevreden and
786 Munro komatiites generally have more variable $\delta^{98}\text{Mo}$ than the spinifex-textured lavas at the
787 same locations (Figs. 1 and S1); with the spinifex-texture samples falling close to the field
788 defined by unaltered magmas undergoing magmatic differentiation. This may presumably be
789 due to a higher proportion of easily altered olivine phenocrysts in the cumulate samples.
790 However, there is no inherent reason why spinifex-texture samples should be less altered than
791 cumulates, one of the spinifex-texture samples measured here has an extremely fractionated
792 $\delta^{98}\text{Mo}$ ($422-99 = +0.007\text{‰}$) and has disturbed Mn/Fe^{2+} . Thus, exclusion for alteration needs
793 to be done on a geochemical rather than rock type basis.

794 The averages presented here for the Weltevreden ($-0.215 \pm 0.038\text{‰}$) and Munro
795 komatiites ($-0.196 \pm 0.044\text{‰}$; Table S3) have are identical within error to those calculated
796 when including all of the Greber, et al.³ data which are $-0.206 \pm 0.071\text{‰}$ ($n = 7$) for
797 Weltevreden and $-0.211 \pm 0.043\text{‰}$ ($n = 9$) for Munro. Inclusion of the previously excluded
798 data also makes little difference to the average composition of Archean komatiites which

799 becomes $-0.204 \pm 0.028\%$ ($n = 20$) and remains resolvably sub-chondritic. In summary,
800 independent of the samples used and the rationale for excluding altered samples the
801 conclusion holds that Archean komatiites are sub-chondritic.

802

803 *The Baffin Island picrites and correlations with $\delta^{98}\text{Mo}$*

804 The fact olivine accumulation controls the major element compositions of the Baffin Island
805 picrites is well established ^{12,53-56}. Here we show Mo concentrations of the Baffin Island
806 samples are strongly correlated with MgO, like many other trace elements (Fig. S3).
807 However, due to the incompatibility of Mo in olivine ($D_{\text{Mo}} = 0.006$ ³⁰), we would expect no
808 effect on $\delta^{98}\text{Mo}$. Previous work by McCoy-West, et al. ¹² showed the Fe and Zn isotope
809 compositions of individual olivines are as light as -0.8% for $\delta^{56}\text{Fe}$ and -0.3% for $\delta^{66}\text{Zn}$,
810 with the bulk rock compositions controlled by the accumulation of variable amounts of
811 olivine that is out of equilibrium with the melt (thus significant kinetic isotope fractionation
812 occurred). A strong covariation between $\delta^{98}\text{Mo}$ and $\delta^{66}\text{Zn}$ (Fig. S4) suggests these variations
813 are controlled by the same process, with correlations also seen versus trace element ratios or
814 elemental concentrations (Fig. S5). Presumably when this diffusional re-equilibration is
815 occurring for Fe and Zn, heavy Mo isotopes were also being preferentially removed from the
816 crystals and entering the melt (all things being equal heavy isotopes prefer the strongest
817 bonds ⁵⁷; i.e. lowest coordination number; see Table S7). Olivines that have then undergone
818 kinetic isotope exchange can then be extremely isotopically light. Variable amounts of these
819 unique olivines are then entrained in subsequent melts and due to the low concentration of
820 Mo in the melt can possibly affect the bulk rock composition.

821

822 From a mass balance standpoint this is hard to envisage due to the extreme
823 incompatibility of Mo in olivine. An alternate scenario is the Mo is hosted within chromite

824 or sulfide inclusions within the olivines. Leaching experiments were conducted on two
825 samples (see Table S9) and the non-silicate (chromite or sulfide) fraction is resolvable
826 isotopically lighter than the residual silicate trapped Mo, this non-silicate fraction also
827 contains ~40 % of the Mo of the samples.

828 Ultimately, the exact nature of this correlation with respect to Mo isotopes is not
829 particularly important for our purposes here. What is important is: 1) the strong linear trends
830 versus a range of different trace element concentrations and ratios (Figs. S4 & S5) shows this
831 is the result of linear addition (i.e. crystal accumulation) rather than magmatic differentiation
832 (where parabolic curves would be expected); and 2) these correlations allow calculation of
833 the composition of the Baffin Island parental melt (Table S2) which is identical within error
834 to all of the other high temperature high degree partial melts measured from 3.5 Ga to the
835 present (Table S3).

836

837 *Estimates of the composition of Mid-ocean ridge basalts*

838 The composition of the MORB mantle is a contentious issue in the Mo isotope scientific
839 literature, with inconsistency between published results^{22,23,46}. Initial work by Hibbert, et al.
840⁵⁸ processed ~1 g of handpicked glasses and obtain $\delta^{98}\text{Mo}$ values of ca. -0.15 to -0.25% . A
841 comprehensive study of MORB glasses by Bezar, et al.²² found the average composition of
842 normal MORB was $-0.180 \pm 0.016\%$ ($n = 18$; as in the main text all errors are 95% s.e.),
843 with the five most depleted samples representative of depleted MORB, uncontaminated by
844 recycled crustal sediments, being slightly sub-chondritic with a an average $\delta^{98}\text{Mo}$ of -0.206
845 $\pm 0.021\%$ ($n = 5$). These studies agree with the average composition of the least altered
846 oceanic crust from ODP site 1256 reported as $-0.20 \pm 0.06\%$ ($n = 5$)⁵⁹. In stark contrast,
847 Liang, et al.²³ found an average MORB composition of $\delta^{98}\text{Mo} = +0.005 \pm 0.025\%$ ($n = 10$).
848 Here we have reanalysed one of the MORB samples presented in Liang, et al.²³ from the

849 North Atlantic Ridge (45N; provided by Kevin Burton in both cases) that had a reported
850 composition of $+0.03 \pm 0.07\%$. Our reanalysis produces an identical Mo concentration of
851 0.41 ppm, but a distinctly different $\delta^{98}\text{Mo}$ value of $-0.159 \pm 0.056\%$ ($n = 2$), which is in
852 agreement with published values for enriched MORBs from the Mohs-Knipovich-Jan Mayen
853 Ridge analysed by Bezar, et al. ²² which range from -0.08 to -0.15% . This new analysis
854 cast doubt over the MORB analyses presented in Liang, et al. ²³. Therefore, in this work we
855 use the published MORB data presented in Bezar, et al. ²². Emphasis here has been placed
856 on the composition of the depleted MORB mantle because a range isotopic studies ⁶⁰⁻⁶² have
857 shown the majority of MORB samples are contaminated by recycled sedimentary material.

858

859 *The composition of the endmembers used in crustal estimate calculations*

860 Modern crustal values of $\delta^{98}\text{Mo}$ and [Mo] are probably not representative of the composition
861 of the early proto-crust, hence here we have modelled a range of crust types using the best
862 estimates of Archean compositions available. The composition of Archean crust can never be
863 determined with certainty, because of the poor preservation of such old rocks ⁴⁸. Indirect
864 approaches, however, suggest the crust was probably dominantly mafic in composition with a
865 subordinate amount of felsic rocks e.g. ^{48-50,63,64}. Following this idea, we created 3 different
866 compositions of Archean crust by mixing different amount of felsic and mafic rocks- *purely*
867 *felsic*, *semi-mafic* and *dominantly-mafic*, which would fully encompass its compositional
868 uncertainty. Clearly the first one is hypothetical, and the latter two are more representative of
869 the Archean crust. For mass balance calculations, we needed two values- elemental, [Mo] and
870 isotopic, $\delta^{98}\text{Mo}$ composition of Mo for the felsic and mafic counterparts (i.e., total four
871 parameters):

872 1) Only [Mo] of Archean felsic rocks (TTGs and granites) are available ¹⁵ which we have
873 used. For all the other parameters, we needed proxies.

874 2) The [Mo] of the basalt endmember (0.155) has been model based on partial melting of the
875 mantle by 30% (sitting in the middle of the Archean range; ^{19,20}) to produce a high Mg basalt
876 using well constrained D values; ^{17,30}. Due to the incompatible nature of Mo, varying the
877 degree of melting from 20 to 40% does not substantial change this value it from 0.23 to 0.12
878 ppm (Fig. S8).

879 3) We chose the $\delta^{98}\text{Mo}$ of average modern basalts (-0.10‰) to represent the mafic
880 endmember. The revised partial melting model shows that melting of a chondritic mantle
881 reservoir to form basalt would reproduce the global basalt average with $\sim 15\%$ melting at
882 1300 °C . This $\sim 0.05\text{ ‰}$ offset is comparable to the natural offset observed between N-
883 MORB ²² and the accessible mantle herein. Melting at higher temperatures or greater degrees
884 of melting would result in a lighter melt. Changing of the composition of the basalt to
885 -0.12‰ (30% melt at 1400 °C) results in a difference in V_{PCC} of only 0.12 (for the 50:50
886 model at 30% mantle depletion), which is smaller than the already displayed error envelopes
887 based on varying endmember composition (see Fig. 4).

888 4) Archean felsic rocks are dominated by TTGs with rare granites (see ⁶⁵ for a review). TTGs
889 are chemically evolved rocks ($\text{SiO}_2 > 65\%$) like granites, but they are primarily characterized
890 by higher Na/K values than true granites. For our purpose, it is important to see what the
891 likely difference in $\delta^{98}\text{Mo}$ between Archean TTGs and modern granites. The elemental
892 concentration of Mo in TTGs and modern and Archean granites are plotted in Figure S7.
893 Phanerozoic granites (Av. Mo = 0.90 ppm) have significantly higher [Mo] than Archean
894 TTGs (Av Mo = 0.28 ppm). Presumably because granites are the result of the multiple
895 episodes of reworking. Therefore, in Figure 4 we present two endmember models, a granite
896 model which provides minimum values of crustal volume and uses the $\delta^{98}\text{Mo}$ of modern
897 granites ($+0.16\text{‰}$) and a TTG model which represents the most realistic estimate based on
898 the available information of the volumes of early crust. Given that TTGs have lower Mo

899 concentrations than granites it is sensible to assume their $\delta^{98}\text{Mo}$ will also be less evolved.
900 Here we have taken the simplest approach (i.e. two step formation of TTGs) and taken the
901 average of global basalts and granites to estimate the $\delta^{98}\text{Mo}$ of TTG felsic component
902 (+0.03‰).

903 There is no *a priori* reason to assume that partial melting processes were different in the
904 Archean than they are today. Therefore, we do not expect significant uncertainties in the
905 crustal volume presented in this study due to the lack of exact match between our chosen
906 proxies for Archean crust and the real Archean crust.

907

908 *The effect of partial melting on Mo isotopes*

909 Two major factors, redox and co-ordination, will control the fractionation of Mo stable
910 isotopes during partial melting e.g. ⁵⁷. Due to the oxidised nature of the terrestrial upper
911 mantle ($\approx\text{FMQ}$), in partial melts of this mantle, Mo predominantly occurs as tetrahedral
912 coordinated Mo^{6+} (MoO_4^{2-}) ^{32,34}. Furthermore, given Mo^{6+} is significantly more incompatible
913 than Mo^{4+} ³⁰ melting products will have higher $\text{Mo}^{6+}/\Sigma\text{Mo}$ than their residue, and hence will
914 be heavier. Co-ordination is a subordinate effect but will also result in an isotopically heavy
915 melt, with Mo in pyroxene (octahedral; ³³ and olivine having higher coordination than in the
916 melt, with heavy isotopes preferentially moving to sites with the lowest coordination number
917 ⁵⁷. The generation of isotopically heavy melts is consistent with the fact average global basalt
918 ($\delta^{98}\text{Mo} = -0.10 \pm 0.04\text{‰}$; ¹⁶), are isotopically heavier than the bulk accessible mantle we
919 observe today ($\delta^{98}\text{Mo} = -0.20 \pm 0.01\text{‰}$; see Table S3). Because Mo is highly incompatible
920 during mantle melting $D_{\text{Mo}} = 0.006\text{-}0.008$ ^{17,30}, it will be quantitatively extracted into the melt
921 except at low degrees of melting (see Fig. S8).

922 Here we have constructed a non-modal batch melting to show the fractionation of Mo
923 isotopes during partial melting based upon the general principles outlined in Sossi and

924 O'Neill³¹. At high degrees of melting as observed in Archean komatiites and the Baffin
925 Island picrites (20-40 % melting), they will remain essential unfractionated from their source
926 region due to the complete removal of Mo from their residue. The corollary is that any Mo
927 remaining in the residual mantle after partial melting is isotopically lighter. At smaller
928 degrees of melting or more reduced conditions the $\Delta^{98}\text{Mo}_{\text{melt-residue}}$ can be larger (see Fig. 3).

929

930 *Alternative estimates of the composition of the bulk silicate Earth*

931 In the main text we have assumed the Mo isotope composition of the bulk silicate Earth
932 (BSE) is the same as the chondritic meteorites Earth accreted from ($\delta^{98}\text{Mo} = -0.154 \pm$
933 0.013‰ ; ^{23,24}). Here we investigate the effects of alternate scenarios on the volume of crust
934 extraction required in the early Earth: 1) the Mo isotope composition of BSE was modified
935 during core formation; or 2) the composition of the BSE is the same as the bulk silicate
936 Moon.

937 **Modification during core formation** (Model 2): The near quantitative removal of Mo to the
938 metallic core means the metallic phase is unlikely to be fractionated from bulk chondrites, as
939 is observed in iron meteorites²⁴. However, this sequestration of Mo may have been
940 associated with a small but resolvable isotopic fractionation of the silicate portion of the
941 planet of up to 0.3‰ ²⁴.

942 When extrapolating to temperatures more closely approximating core formation ($>2000\text{ °C}$
943 ⁶⁶) initial metal-silicate equilibration experiments⁶⁷ suggested a resolvable $\Delta^{98}\text{Mo}_{\text{metal-silicate}}$ of
944 -0.052‰ at 2500 °C , but subsequent work which incorporates the effect of Mo valance state
945 ⁶⁸ suggests a significantly reduced $\Delta^{98}\text{Mo}_{\text{metal-silicate}}$ of as little as -0.008‰ (assuming reduced
946 conditions with $\text{Mo}^{6+}/\Sigma\text{Mo} = 0.1$). This parameterization requires accurate knowledge of
947 both the temperature and oxygen fugacity at the time of core formation, neither of which we
948 know with certainty. However, we can make an educated estimate on the maximum effect of
949 core formation. Core formation is expected to occur between 2000 °C and 3000 °C ^{66,69-71}

950 and requires highly reduced conditions initially^{66,72}. A reasonable upper estimate of the
951 maximum effect of core formation could impart is $\Delta_{98\text{Mo metal-silicate}} = -0.012\text{‰}$ (assuming $T =$
952 2000 °C ; $\text{Mo}^{6+}/\Sigma\text{Mo} = 0.1$), meaning that if the mantle is indeed isotopically heavier it will
953 still be within error of the composition of chondrites. Crustal volume estimates based on an
954 isotopically heavier BSE following core formation ($\delta^{98}\text{Mo} = -0.142\text{‰}$) are presented in
955 Figure S6 (c-d). These estimates are higher (3.4-5.3 times PVCC) but not drastically
956 different than the modelling assuming a chondritic BSE.

957 **Composition similar to bulk silicate Moon (Model 3):** We also explored the effect of a BSE
958 composition based on the Earth-Moon equilibration as done by Willbold and Elliott⁴⁶. This
959 idea is based on assuming the BSE and Moon were once isotopically equilibrated as has been
960 shown for several lithophile elements^{73,74}. Using analyses of lunar samples ($\delta^{98}\text{Mo} = -0.050$
961 $\pm 0.033\text{‰}$;²⁴), and assuming subsequent late accretion of 1% chondritic material results in a
962 $\delta^{98}\text{Mo}$ of -0.078‰ . By using this value for the BSE and then undertaking mass balance
963 modelling to investigate the volume of crust, generates unrealistically large volumes of crust
964 (Fig. S6e-f). Namely, using TTG felsic materials for mafic crust-A (50:50 mafic-felsic rocks)
965 and a depleted mantle comprising 30% of the mantle would require 14 times the PVCC. This
966 value is even higher for the mafic crust-B (75:25 mafic-felsic rocks). Requiring >10 times the
967 PVCC is highly unrealistic, considering the recycling rates and present extent of crustal
968 volume. Therefore, for Mo it is extremely unlikely that the BSE was ever fully equilibrated
969 with the bulk silicate Moon.

970

971 *The effect of the lower crust*

972 On the modern Earth the continental crust has a well-developed lower crust^{48,63,64}. Estimates
973 of the composition of the continental crust from molybdenites, granites and arc-related
974 basalts are consistent with a super-chondritic $\delta^{98}\text{Mo}$ from $+0.05$ to $+0.30\text{‰}$ ^{16,75,76}. These

975 archives are focused on the upper continental crust (arc basalts are a record of juvenile
976 continental crust), but do not consider the effect of possible compositional variations in the
977 lower crust. However, given the extreme incompatibility of Mo during mantle melting $D_{\text{Mo}} =$
978 $0.006-0.008$ ^{17,30}, Mo essentially becomes concentrated in the upper crust rather than any
979 lower crustal cumulates. An additional complication would be the presence of residual
980 sulfides, that due to its chalcophile behaviour will preferentially incorporate Mo. However,
981 given on the modern Earth most continental crust is predominantly formed in subduction-like
982 environments sulfide-saturation will generally be delayed (due to higher $f\text{O}_2$, and water
983 contents), and therefore Mo will remain in the melt phase and removed to the upper crust.

984 The composition and makeup of the Archean crust was not identical to modern crust
985 ^{48,63,64}. Therefore, whether the Archean crust has a well-defined lower crust similar to today
986 or not is unknown. Instead, studies infer that the whole Archean crust was dominantly mafic
987 and may have contained subordinate amount of granitoids ^{49,50,63}. We have considered this
988 factor while carrying out the mass balance modelling by using 3 different crustal
989 compositions: (1) purely felsic (100% granitoids); (2) semi-mafic (Mafic crust-A;
990 combination of mafic-felsic in 50:50); and (3) dominantly-mafic (Mafic crust-B; with a
991 mafic-felsic ratio of 75:25). The mafic component of the latter two crustal types is
992 approximated from the Mo isotope composition of global average of basalts (juvenile melt).
993 Now, TTGs form when these basalts get metamorphosed and partially melted at amphibolite
994 or eclogite facies e.g. ^{77,78}. Therefore, we should expect a depleted residual mass in the lower
995 crust complementing the TTG composition. But, this depleted lower crust is extremely
996 unlikely to remain preserved in the crust, due to the geodynamic setting where Hadean to
997 early Archean TTGs are inferred to have formed (i.e. a stagnant-lid regime: either when the
998 meta-basalts drip back into the mantle (delamination) or during the mantle lid overturn events
999 that recycle the pre-existing crust back to the mantle ^{65,78-80}). The crucial point is, the

1000 preserved crustal profile is largely devoid of residues formed after TTG extraction. Therefore,
1001 the crust is dominated by juvenile, melt-undepleted (meta-)basalts and granitoids. As stated
1002 above, our existing mass balance calculations consider both these components of the Archean
1003 crust as realistically as possible. Furthermore, even if some fraction of this TTG-depleted
1004 residual mass remains in the crust, it is likely to be of granulite to eclogite grade- where rutile
1005 exists ⁷⁷. It has been shown that in such cases, rutile should dominate the Mo-budget ^{15,81,82}.
1006 Mo-concentration within such eclogitic rutile can vary within 2-7 ppm ⁸² and thermodynamic
1007 phase equilibria modelling suggests that the Archean meta-basalts would have contained not
1008 more than ~0.5 volume % of rutile ⁸³. In that case, the net Mo concentration will not deviate
1009 much from that of average basalt, which we have already considered for the mafic component
1010 of our model crustal types. This further attest that the crustal volume range bracketed by
1011 semi-mafic and dominantly-mafic crustal types potentially accounts for the variations due to
1012 any depleted lower crustal rocks.
1013

1014 **References**

- 1015 1 Hibbert, K. E. J., Williams, H. M., Kerr, A. C. & Puchtel, I. S. Iron isotopes in ancient and modern
1016 komatiites: Evidence in support of an oxidised mantle from Archean to present. *Earth and Planetary*
1017 *Science Letters* **321–322**, 198-207, doi:<http://dx.doi.org/10.1016/j.epsl.2012.01.011> (2012).
- 1018 2 Dauphas, N., Teng, F.-Z. & Arndt, N. T. Magnesium and iron isotopes in 2.7 Ga Alexo komatiites:
1019 Mantle signatures, no evidence for Soret diffusion, and identification of diffusive transport in zoned
1020 olivine. *Geochimica et Cosmochimica Acta* **74**, 3274-3291,
1021 doi:<https://doi.org/10.1016/j.gca.2010.02.031> (2010).
- 1022 3 Greber, N. D., Puchtel, I. S., Nägler, T. F. & Mezger, K. Komatiites constrain molybdenum isotope
1023 composition of the Earth's mantle. *Earth and Planetary Science Letters* **421**, 129-138,
1024 doi:<https://doi.org/10.1016/j.epsl.2015.03.051> (2015).
- 1025 4 DePaolo, D. J., Linn, A. M. & Schubert, G. The continental crustal age distribution: Methods of
1026 determining mantle separation ages from Sm-Nd isotopic data and application to the southwestern
1027 United States. *Journal of Geophysical Research: Solid Earth* **96**, 2071-2088, doi:10.1029/90jb02219
1028 (1991).
- 1029 5 Puchtel, I. S., Humayun, M., Campbell, A. J., Sproule, R. A. & Leshner, C. M. Platinum group element
1030 geochemistry of komatiites from the Alexo and Pyke Hill areas, Ontario, Canada 11Associate editor: R.
1031 J. Walker. *Geochimica et Cosmochimica Acta* **68**, 1361-1383,
1032 doi:<https://doi.org/10.1016/j.gca.2003.09.013> (2004).
- 1033 6 Puchtel, I. S. *et al.* Insights into early Earth from Barberton komatiites: Evidence from lithophile
1034 isotope and trace element systematics. *Geochimica et Cosmochimica Acta* **108**, 63-90,
1035 doi:<https://doi.org/10.1016/j.gca.2013.01.016> (2013).
- 1036 7 Starkey, N. A. *et al.* Helium isotopes in early Iceland plume picrites: Constraints on the composition of
1037 high 3He/4He mantle. *Earth and Planetary Science Letters* **277**, 91-100,
1038 doi:<https://doi.org/10.1016/j.epsl.2008.10.007> (2009).
- 1039 8 Sossi, P. A. *et al.* Petrogenesis and Geochemistry of Archean Komatiites. *Journal of Petrology* **57**, 147-
1040 184, doi:10.1093/petrology/egw004 (2016).
- 1041 9 Kerr, A. C. La Isla de Gorgona, Colombia: A petrological enigma? *Lithos* **84**, 77-101,
1042 doi:<http://dx.doi.org/10.1016/j.lithos.2005.02.006> (2005).
- 1043 10 Jacobsen, S. B. Isotopic and chemical constraints on mantle-crust evolution. *Geochimica et*
1044 *Cosmochimica Acta* **52**, 1341-1350, doi:[https://doi.org/10.1016/0016-7037\(88\)90205-0](https://doi.org/10.1016/0016-7037(88)90205-0) (1988).
- 1045 11 Jacobsen, S. B. & Wasserburg, G. J. The mean age of mantle and crustal reservoirs. *Journal of*
1046 *Geophysical Research: Solid Earth* **84**, 7411-7427, doi:doi:10.1029/JB084iB13p07411 (1979).
- 1047 12 McCoy-West, A. J., Godfrey Fitton, J., Pons, M.-L., Inglis, E. C. & Williams, H. M. The Fe and Zn
1048 isotope composition of deep mantle source regions: Insights from Baffin Island picrites. *Geochimica et*
1049 *Cosmochimica Acta* **238**, 542-562, doi:<https://doi.org/10.1016/j.gca.2018.07.021> (2018).
- 1050 13 DePaolo, D. J. Crustal growth and mantle evolution: inferences from models of element transport and
1051 Nd and Sr isotopes. *Geochimica et Cosmochimica Acta* **44**, 1185-1196,
1052 doi:[https://doi.org/10.1016/0016-7037\(80\)90072-1](https://doi.org/10.1016/0016-7037(80)90072-1) (1980).
- 1053 14 O'Nions, R. K., Evensen, N. M. & Hamilton, P. J. Geochemical modeling of mantle differentiation and
1054 crustal growth. *Journal of Geophysical Research: Solid Earth* **84**, 6091-6101,
1055 doi:doi:10.1029/JB084iB11p06091 (1979).
- 1056 15 Greaney, A. T. *et al.* Geochemistry of molybdenum in the continental crust. *Geochimica et*
1057 *Cosmochimica Acta* **238**, 36-54, doi:<https://doi.org/10.1016/j.gca.2018.06.039> (2018).
- 1058 16 Yang, J. *et al.* The molybdenum isotopic compositions of I-, S- and A-type granitic suites. *Geochimica*
1059 *et Cosmochimica Acta* **205**, 168-186, doi:<https://doi.org/10.1016/j.gca.2017.01.027> (2017).
- 1060 17 Wang, Z. & Becker, H. Molybdenum partitioning behavior and content in the depleted mantle: Insights
1061 from Balmuccia and Baldissero mantle tectonites (Ivrea Zone, Italian Alps). *Chemical Geology* **499**,
1062 138-150, doi:<https://doi.org/10.1016/j.chemgeo.2018.09.023> (2018).
- 1063 18 Palme, H. & O'Neill, H. S. C. in *Treatise on Geochemistry (Second Edition)* (eds Heinrich D. Holland
1064 & Karl K. Turekian) 1-39 (Elsevier, 2014).
- 1065 19 Herzberg, C., Condie, K. & Korenaga, J. Thermal history of the Earth and its petrological expression.
1066 *Earth and Planetary Science Letters* **292**, 79-88, doi:<https://doi.org/10.1016/j.epsl.2010.01.022> (2010).
- 1067 20 Keller, C. B. & Schoene, B. Statistical geochemistry reveals disruption in secular lithospheric evolution
1068 about 2.5 Gyr ago. *Nature* **485**, 490, doi:10.1038/nature11024
1069 <https://www.nature.com/articles/nature11024#supplementary-information> (2012).
- 1070 21 Isoplot 3.71 v. 3.71 (Berkeley Geochronology Centre, 2008).
- 1071 22 Bezaud, R., Fischer-Gödde, M., Hamelin, C., Brennecke, G. A. & Kleine, T. The effects of magmatic
1072 processes and crustal recycling on the molybdenum stable isotopic composition of Mid-Ocean Ridge

1073 Basalts. *Earth and Planetary Science Letters* **453**, 171-181,
1074 doi:<http://dx.doi.org/10.1016/j.epsl.2016.07.056> (2016).

1075 23 Liang, Y.-H. *et al.* Molybdenum isotope fractionation in the mantle. *Geochimica et Cosmochimica*
1076 *Acta* **199**, 91-111, doi:<https://doi.org/10.1016/j.gca.2016.11.023> (2017).

1077 24 Burkhardt, C., Hin, R. C., Kleine, T. & Bourdon, B. Evidence for Mo isotope fractionation in the solar
1078 nebula and during planetary differentiation. *Earth and Planetary Science Letters* **391**, 201-211,
1079 doi:<http://dx.doi.org/10.1016/j.epsl.2014.01.037> (2014).

1080 25 Yoder, C. F. in *Global Earth Physics: A Handbook of Physical Constants* Vol. AGU Reference Shelf
1081 (ed T. J. Ahrens) pp. 1-31 (American Geophysical Union., 1995).

1082 26 McDonough, W. F. in *Treatise on Geochemistry (First Edition)* Vol. 2 (eds Heinrich D. Holland &
1083 Karl K. Turekian) 547-568 (Elsevier, 2003).

1084 27 Salters, V. J. M. & Stracke, A. Composition of the depleted mantle. *Geochemistry, Geophysics,*
1085 *Geosystems* **5**, doi:doi:10.1029/2003GC000597 (2004).

1086 28 Rudnick, R. L. & Gao, S. in *Treatise on Geochemistry (Second Edition)* (eds Heinrich D. Holland &
1087 Karl K. Turekian) 1-51 (Elsevier, 2014).

1088 29 Walter, M. J. in *Treatise of Geochemistry* Vol. 2.08 (ed R. W. Carlson) 363-394 (Elsevier, 2003).

1089 30 Leitzke, F. P. *et al.* Redox dependent behaviour of molybdenum during magmatic processes in the
1090 terrestrial and lunar mantle: Implications for the Mo/W of the bulk silicate Moon. *Earth and Planetary*
1091 *Science Letters* **474**, 503-515, doi:<https://doi.org/10.1016/j.epsl.2017.07.009> (2017).

1092 31 Sossi, P. A. & O'Neill, H. S. C. The effect of bonding environment on iron isotope fractionation
1093 between minerals at high temperature. *Geochimica et Cosmochimica Acta* **196**, 121-143,
1094 doi:<https://doi.org/10.1016/j.gca.2016.09.017> (2017).

1095 32 O'Neill, H. S. C. & Eggins, S. M. The effect of melt composition on trace element partitioning: an
1096 experimental investigation of the activity coefficients of FeO, NiO, CoO, MoO₂ and MoO₃ in silicate
1097 melts. *Chemical Geology* **186**, 151-181, doi:[http://dx.doi.org/10.1016/S0009-2541\(01\)00414-4](http://dx.doi.org/10.1016/S0009-2541(01)00414-4) (2002).

1098 33 Adam, J. & Green, T. Trace element partitioning between mica- and amphibole-bearing garnet
1099 lherzolite and hydrous basanitic melt: 1. Experimental results and the investigation of controls on
1100 partitioning behaviour. *Contributions to Mineralogy and Petrology* **152**, 1-17, doi:10.1007/s00410-
1101 006-0085-4 (2006).

1102 34 Farges, F. o., Siewert, R., Brown, J. G. E., Guesdon, A. & Morin, G. Structural environments around
1103 molybdenum in silicate glasses and melts. I. Influence of composition and oxygen fugacity on the local
1104 structure of molybdenum. *The Canadian Mineralogist* **44**, 731-753, doi:10.2113/gscanmin.44.3.731
1105 (2006).

1106 35 Starkey, N. A. *Evolution of the Earth's mantle-crust-atmosphere system from the trace element and*
1107 *isotope geochemistry of the plume-mantle reservoir* PhD thesis, Ph.D. thesis, University of Edinburgh,
1108 (2009).

1109 36 Sossi, P. A., Nebel, O., O'Neill, H. S. C. & Moynier, F. Zinc isotope composition of the Earth and its
1110 behaviour during planetary accretion. *Chemical Geology* **477**, 73-84,
1111 doi:<https://doi.org/10.1016/j.chemgeo.2017.12.006> (2018).

1112 37 Rudge, J. F., Reynolds, B. C. & Bourdon, B. The double spike toolbox. *Chemical Geology* **265**, 420-
1113 431, doi:<http://dx.doi.org/10.1016/j.chemgeo.2009.05.010> (2009).

1114 38 Willbold, M. *et al.* High-Precision Mass-Dependent Molybdenum Isotope Variations in Magmatic
1115 Rocks Determined by Double-Spike MC-ICP-MS. *Geostandards and Geoanalytical Research* **40**, 389-
1116 403, doi:10.1111/j.1751-908X.2015.00388.x (2016).

1117 39 Greber, N. D., Siebert, C., Nägler, T. F. & Pettke, T. $\delta^{98/95}\text{Mo}$ values and Molybdenum Concentration
1118 Data for NIST SRM 610, 612 and 3134: Towards a Common Protocol for Reporting Mo Data.
1119 *Geostandards and Geoanalytical Research* **36**, 291-300, doi:10.1111/j.1751-908X.2012.00160.x
1120 (2012).

1121 40 Goldberg, T. *et al.* Resolution of inter-laboratory discrepancies in Mo isotope data: an intercalibration.
1122 *Journal of Analytical Atomic Spectrometry* **28**, 724-735, doi:10.1039/c3ja30375f (2013).

1123 41 Creech, J. B. & Paul, B. IsoSpike: Improved Double-Spike Inversion Software. *Geostandards and*
1124 *Geoanalytical Research* **39**, 7-15, doi:10.1111/j.1751-908X.2014.00276.x (2015).

1125 42 Paton, C., Hellstrom, J., Paul, B., Woodhead, J. & Hergt, J. Iolite: Freeware for the visualisation and
1126 processing of mass spectrometric data. *Journal of Analytical Atomic Spectrometry* **26**, 2508-2518
1127 (2011).

1128 43 Neely, R. A. *et al.* Molybdenum isotope behaviour in groundwaters and terrestrial hydrothermal
1129 systems, Iceland. *Earth and Planetary Science Letters* **486**, 108-118, doi:10.1016/j.epsl.2017.11.053
1130 (2018).

- 1131 44 Zhao, P.-P. *et al.* Molybdenum Mass Fractions and Isotopic Compositions of International Geological
1132 Reference Materials. *Geostandards and Geoanalytical Research* **40**, 217-226, doi:10.1111/j.1751-
1133 908X.2015.00373.x (2015).
- 1134 45 Yang, J. *et al.* Absence of molybdenum isotope fractionation during magmatic differentiation at Hekla
1135 volcano, Iceland. *Geochimica et Cosmochimica Acta* **162**, 126-136,
1136 doi:<http://dx.doi.org/10.1016/j.gca.2015.04.011> (2015).
- 1137 46 Willbold, M. & Elliott, T. Molybdenum isotope variations in magmatic rocks. *Chemical Geology* **449**,
1138 253-268, doi:<https://doi.org/10.1016/j.chemgeo.2016.12.011> (2017).
- 1139 47 Hofmann, A. W. Mantle geochemistry: the message from oceanic volcanism. *Nature* **385**, 219,
1140 doi:10.1038/385219a0 (1997).
- 1141 48 Cawood, P. A., Hawkesworth, C. J. & Dhuime, B. The continental record and the generation of
1142 continental crust. *GSA Bulletin* **125**, 14-32, doi:10.1130/B30722.1 (2013).
- 1143 49 Dhuime, B., Wuestefeld, A. & Hawkesworth, C. J. Emergence of modern continental crust about 3
1144 billion years ago. *Nature Geoscience* **8**, 552, doi:10.1038/ngeo2466
1145 <https://www.nature.com/articles/ngeo2466#supplementary-information> (2015).
- 1146 50 Tang, M., Chen, K. & Rudnick, R. L. Archean upper crust transition from mafic to felsic marks the
1147 onset of plate tectonics. *Science* **351**, 372-375, doi:10.1126/science.aad5513 (2016).
- 1148 51 Bali, E., Keppler, H. & Audetat, A. The mobility of W and Mo in subduction zone fluids and the Mo-
1149 W-Th-U systematics of island arc magmas. *Earth and Planetary Science Letters* **351-352**, 195-207,
1150 doi:<http://dx.doi.org/10.1016/j.epsl.2012.07.032> (2012).
- 1151 52 Keppler, H. & Wyllie, P. J. Partitioning of Cu, Sn, Mo, W, U, and Th between melt and aqueous fluid
1152 in the systems haplogranite-H₂O-HCl and haplogranite-H₂O-HF. *Contributions to Mineralogy and
1153 Petrology* **109**, 139-150, doi:10.1007/bf00306474 (1991).
- 1154 53 Clarke, D. B. Tertiary basalts of Baffin Bay: Possible primary magma from the mantle. *Contributions
1155 to Mineralogy and Petrology* **25**, 203-224, doi:10.1007/bf00371131 (1970).
- 1156 54 Francis, D. The Baffin Bay lavas and the value of picrites as analogues of primary magmas.
1157 *Contributions to Mineralogy and Petrology* **89**, 144-154, doi:10.1007/BF00379449 (1985).
- 1158 55 Larsen, L. M. & Pedersen, A. K. Processes in high-Mg, high-T magmas: Evidence from olivine,
1159 chromite and glass in Palaeogene picrites from West Greenland. *Journal of Petrology* **41**, 1071-1098,
1160 doi:10.1093/petrology/41.7.1071 (2000).
- 1161 56 Starkey, N. A., Fitton, J. G., Stuart, F. M. & Larsen, L. M. Melt inclusions in olivines from early
1162 Iceland plume picrites support high 3He/4He in both enriched and depleted mantle. *Chemical Geology*
1163 **306-307**, 54-62, doi:<https://doi.org/10.1016/j.chemgeo.2012.02.022> (2012).
- 1164 57 Schauble, E. A. Applying Stable Isotope Fractionation Theory to New Systems. *Reviews in Mineralogy
1165 and Geochemistry* **55**, 65-111 (2004).
- 1166 58 Hibbert, K., Freymuth, H., Willbold, M. & Elliott, T. Mass-dependent molybdenum isotopes in mid-
1167 ocean ridge basalts: A new mantle reference. *American Geophysical Union Fall Meeting San
1168 Francisco, California*, Abstract V52A-04 (2013).
- 1169 59 Freymuth, H., Vils, F., Willbold, M., Taylor, R. N. & Elliott, T. Molybdenum mobility and isotopic
1170 fractionation during subduction at the Mariana arc. *Earth and Planetary Science Letters* **432**, 176-186,
1171 doi:<http://dx.doi.org/10.1016/j.epsl.2015.10.006> (2015).
- 1172 60 Nielsen, S. G. *et al.* Barium isotope evidence for pervasive sediment recycling in the upper mantle.
1173 *Science Advances* **4**, doi:10.1126/sciadv.aas8675 (2018).
- 1174 61 Andersen, M. B. *et al.* The terrestrial uranium isotope cycle. *Nature* **517**, 356, doi:10.1038/nature14062
1175 <https://www.nature.com/articles/nature14062#supplementary-information> (2015).
- 1176 62 Rehkamper, M. & Hofmann, A. W. Recycled ocean crust and sediment in Indian Ocean MORB. *Earth
1177 and Planetary Science Letters* **147**, 93-106, doi:[https://doi.org/10.1016/S0012-821X\(97\)00009-5](https://doi.org/10.1016/S0012-821X(97)00009-5)
1178 (1997).
- 1179 63 Kamber, B. S., Whitehouse, M. J., Bolhar, R. & Moorbath, S. Volcanic resurfacing and the early
1180 terrestrial crust: Zircon U-Pb and REE constraints from the Isua Greenstone Belt, southern West
1181 Greenland. *Earth and Planetary Science Letters* **240**, 276-290,
1182 doi:<https://doi.org/10.1016/j.epsl.2005.09.037> (2005).
- 1183 64 Cawood, P. A. *et al.* Geological archive of the onset of plate tectonics. *Philosophical Transactions of
1184 the Royal Society A: Mathematical, Physical and Engineering Sciences* **376**, 20170405,
1185 doi:10.1098/rsta.2017.0405 (2018).
- 1186 65 Moyen, J.-F. & Laurent, O. Archean tectonic systems: A view from igneous rocks. *Lithos* **302-303**,
1187 99-125, doi:<https://doi.org/10.1016/j.lithos.2017.11.038> (2018).
- 1188 66 Wade, J. & Wood, B. J. Core formation and the oxidation state of the Earth. *Earth and Planetary
1189 Science Letters* **236**, 78-95, doi:<https://doi.org/10.1016/j.epsl.2005.05.017> (2005).

1190 67 Hin, R. C., Burkhardt, C., Schmidt, M. W., Bourdon, B. & Kleine, T. Experimental evidence for Mo
1191 isotope fractionation between metal and silicate liquids. *Earth and Planetary Science Letters* **379**, 38-
1192 48, doi:<http://dx.doi.org/10.1016/j.epsl.2013.08.003> (2013).

1193 68 Hin, R. C., Burnham, A. D., Gianolio, D., Walter, M. J. & Elliott, T. Molybdenum isotope fractionation
1194 between Mo⁴⁺ and Mo⁶⁺ in silicate liquid and metallic Mo. *Chemical Geology* **504**, 177-189,
1195 doi:<https://doi.org/10.1016/j.chemgeo.2018.11.014> (2019).

1196 69 Siebert, J., Corgne, A. & Ryerson, F. J. Systematics of metal–silicate partitioning for many siderophile
1197 elements applied to Earth’s core formation. *Geochimica et Cosmochimica Acta* **75**, 1451-1489,
1198 doi:<https://doi.org/10.1016/j.gca.2010.12.013> (2011).

1199 70 Righter, K., Pando, K. M., Danielson, L. & Lee, C.-T. Partitioning of Mo, P and other siderophile
1200 elements (Cu, Ga, Sn, Ni, Co, Cr, Mn, V, and W) between metal and silicate melt as a function of
1201 temperature and silicate melt composition. *Earth and Planetary Science Letters* **291**, 1-9,
1202 doi:<http://dx.doi.org/10.1016/j.epsl.2009.12.018> (2010).

1203 71 Ballhaus, C. *et al.* The U/Pb ratio of the Earth's mantle—A signature of late volatile addition. *Earth
1204 and Planetary Science Letters* **362**, 237-245, doi:<https://doi.org/10.1016/j.epsl.2012.11.049> (2013).

1205 72 Wade, J., Wood, B. J. & Tuff, J. Metal–silicate partitioning of Mo and W at high pressures and
1206 temperatures: Evidence for late accretion of sulphur to the Earth. *Geochimica et Cosmochimica Acta*
1207 **85**, 58-74, doi:<http://dx.doi.org/10.1016/j.gca.2012.01.010> (2012).

1208 73 Armytage, R. M. G., Georg, R. B., Williams, H. M. & Halliday, A. N. Silicon isotopes in lunar rocks:
1209 Implications for the Moon’s formation and the early history of the Earth. *Geochimica et Cosmochimica
1210 Acta* **77**, 504-514, doi:<https://doi.org/10.1016/j.gca.2011.10.032> (2012).

1211 74 Young, E. D. *et al.* Oxygen isotopic evidence for vigorous mixing during the Moon-forming giant
1212 impact. *Science* **351**, 493, doi:10.1126/science.aad0525 (2016).

1213 75 Voegelin, A. R., Pettke, T., Greber, N. D., von Niederhäusern, B. & Nägler, T. F. Magma
1214 differentiation fractionates Mo isotope ratios: Evidence from the Kos Plateau Tuff (Aegean Arc).
1215 *Lithos* **190–191**, 440-448, doi:<http://dx.doi.org/10.1016/j.lithos.2013.12.016> (2014).

1216 76 Greber, N. D., Pettke, T. & Nägler, T. F. Magmatic–hydrothermal molybdenum isotope fractionation
1217 and its relevance to the igneous crustal signature. *Lithos* **190-191**, 104-110,
1218 doi:<https://doi.org/10.1016/j.lithos.2013.11.006> (2014).

1219 77 Moyen, J.-F. & Martin, H. Forty years of TTG research. *Lithos* **148**, 312-336,
1220 doi:<http://dx.doi.org/10.1016/j.lithos.2012.06.010> (2012).

1221 78 Johnson, T. E., Brown, M., Gardiner, N. J., Kirkland, C. L. & Smithies, R. H. Earth’s first stable
1222 continents did not form by subduction. *Nature* **543**, 239, doi:10.1038/nature21383
1223 <https://www.nature.com/articles/nature21383#supplementary-information> (2017).

1224 79 Sizova, E., Gerya, T., Stüwe, K. & Brown, M. Generation of felsic crust in the Archean: A geodynamic
1225 modeling perspective. *Precambrian Research* **271**, 198-224,
1226 doi:<https://doi.org/10.1016/j.precamres.2015.10.005> (2015).

1227 80 Rozel, A. B., Golabek, G. J., Jain, C., Tackley, P. J. & Gerya, T. Continental crust formation on early
1228 Earth controlled by intrusive magmatism. *Nature* **545**, 332, doi:10.1038/nature22042 (2017).

1229 81 Fitton, J. G. Coupled molybdenum and niobium depletion in continental basalts. *Earth and Planetary
1230 Science Letters* **136**, 715-721, doi:[https://doi.org/10.1016/0012-821X\(95\)00171-8](https://doi.org/10.1016/0012-821X(95)00171-8) (1995).

1231 82 Zack, T., Kronz, A., Foley, S. F. & Rivers, T. Trace element abundances in rutiles from eclogites and
1232 associated garnet mica schists. *Chemical Geology* **184**, 97-122, doi:[https://doi.org/10.1016/S0009-
1233 2541\(01\)00357-6](https://doi.org/10.1016/S0009-2541(01)00357-6) (2002).

1234 83 Johnson, T. E., Brown, M., Kaus, B. J. P. & VanTongeren, J. A. Delamination and recycling of
1235 Archaean crust caused by gravitational instabilities. *Nature Geoscience* **7**, 47, doi:10.1038/ngeo2019
1236 <https://www.nature.com/articles/ngeo2019#supplementary-information> (2013).

1237

1238